10710
NACA TN 4366

TECH LIBRARY KAFB, NM
0067168

NATIONAL ADVISORY COMMITTEE FOR AERONAUTICS

TECHNICAL NOTE 4366

THE EFFECTS OF AN INVERSE-TAPER LEADING-EDGE FLAP ON THE AERODYNAMIC CHARACTERISTICS IN PITCH OF A WING-BODY COMBINATION HAVING AN ASPECT RATIO OF 3 AND 45° OF SWEEPBACK AT MACH NUMBERS TO 0.92

By Fred A. Demele and K. Harmon Powell

Ames Aeronautical Laboratory
Moffett Field, Calif.

Washington
August 1958

AFMDC
TECHNICAL LIBRARY
AFL 2811

TECH LIBRARY KAFB, NM
0067168

NATIONAL ADVISORY COMMITTEE FOR AERONAUTICS

TECHNICAL NOTE 4366

THE EFFECTS OF AN INVERSE-TAPER LEADING-EDGE FLAP ON THE AERODYNAMIC CHARACTERISTICS IN PITCH OF A WING-BODY COMBINATION HAVING AN ASPECT RATIO OF 3 and 45° OF SWEEPBACK AT MACH NUMBERS TO 0.92

By Fred A. Demele and K. Harmon Powell

SUMMARY

An investigation has been made to determine the effects of an inverse-taper leading-edge flap on the drag and on the static-longitudinal characteristics of a swept-wing-body combination. The wing had 45° of leading-edge sweepback, an aspect ratio of 3, a taper ratio of 0.4, and no camber or twist. However, with the flap deflected, the wing had a camber and twist distribution similar to that resulting from the incorporation of conical camber in the forward portion of a plane wing. The tests were conducted over a range of Mach numbers from 0.25 to 0.92 at a Reynolds number of 3.2 million, and over a Reynolds number range of 3.2 million to 15 million at a Mach number of 0.25 with flap deflections to 16°.

In the range of Mach numbers from 0.60 to 0.92, deflection of the flap resulted in significant drag reductions at lift coefficients of 0.2 and greater. For optimum flap deflection, the maximum lift-drag ratios were near the estimated maximums based on the assumptions of elliptic span loading and full leading-edge suction. Slightly higher increases in maximum lift-drag ratio were associated with optimum flap deflection than with conical camber. At a Mach number of 0.25 and at a Reynolds number of 15 million the flap was effective in reducing drag only at lift coefficients above 0.55. In general, the flap had little effect on the lift and static stability of the model.

INTRODUCTION

For certain missions of airplanes capable of supersonic flight, it may be most economical to cruise at high subsonic speeds. Thus, it is important that the subsonic lift-drag ratios be maximized with minimum penalty to the supersonic capabilities of the airplane. Supersonic flight necessitates the use of thin wings which are not conducive to high

aerodynamic efficiency at subsonic speeds. The usual leading-edge shape of such wings causes separation to occur at a low lift coefficient and consequently prevents the attainment, above that lift coefficient, of an effective leading-edge suction force necessary for low drag due to lift. It was shown in references 1 and 2 that it is possible to attain very low values of drag due to lift at subsonic speeds by incorporating conical camber over the forward portion of thin wings, even though such camber is designed for low supersonic speeds. Cambering in this manner causes the leading-edge suction pressures (i.e., pressures less than free-stream static) to be distributed over a larger area. Hence, to produce the leading-edge suction effect required for low drag due to lift, these pressures need not be as low as if they were concentrated at the leading edge and are therefore physically realizable. Although large improvements in maximum lift-drag ratio at high subsonic speeds resulted from cambering a wing in this manner, there were small minimum drag penalties associated with the camber at supersonic speeds. Since a plane wing has lower minimum drag at supersonic speeds, it was considered desirable to determine whether the subsonic benefits of this type of camber could be achieved with a plane wing having an inverse-taper leading-edge flap which, in the deflected position, would result in a camber and twist distribution approximating the conical type. It was reasoned that such a configuration would permit greater performance flexibility throughout the entire speed regime than a wing having fixed camber.

The present investigation was therefore undertaken to determine the effects of an inverse-taper leading-edge flap on the drag and static longitudinal characteristics of a swept-wing-body combination. The wing plan form and thickness distribution were identical to those employed in the conical cambered wings of reference 2. The wing had 45° of sweepback of the leading edge, an aspect ratio of 3, a taper ratio of 0.4, and streamwise sections approximately 5 percent thick. The tests were conducted in the Ames 12-foot pressure wind tunnel over a Mach number range from 0.25 to 0.92 at a Reynolds number of 3.2×10^{6}, and over a Reynolds number range from 3.2×10^{6} to 15×10^{6} at a Mach number of 0.25.

NOTATION

A aspect ratio

b span

c wing chord

$\bar{c}$ wing mean aerodynamic chord

C_D drag coefficient, $\frac{\text{drag}}{qS}$

C_{L_d} design lift coefficient

C_L lift coefficient, $\frac{\text{lift}}{qS}$

C_m pitching-moment coefficient, $\frac{\text{pitching moment}}{qS\bar{c}}$, referred to quarter point of the mean aerodynamic chord

D drag

L lift

L.E. leading edge

M free-stream Mach number

q free-stream dynamic pressure

R Reynolds number, based on the wing mean aerodynamic chord

S area of semispan wing

x longitudinal distance from wing leading edge

y lateral distance from plane of symmetry

z vertical distance from wing chord plane

α angle of attack, measured with respect to the wing chord at the plane of symmetry

δ flap angle in a direction parallel to the plane of symmetry (see fig. 2)

$\frac{dC_L}{d\alpha}$ lift-curve slope in the vicinity of $C_L = 0$

$\frac{dC_m}{dC_L}$ pitching-moment-curve slope in the vicinity of $C_L = 0$

Subscripts

max maximum

opt optimum

o zero lift

MODEL

The semispan model used in this investigation consisted of the right wing panel of a sweptback wing mounted in a midwing position on a half body. The model was mounted on a turntable in the floor of the wind tunnel as shown in figure 1, with the turntable supported on a lever-type balance. The wing, which was constructed of Fiberglas over a steel spar, had 45° sweepback of the leading edge, an aspect ratio of 3, and a taper ratio of 0.4. The sections normal to the quarter-chord line had modified NACA 64A006 profiles, the modification consisting of increased leading-edge radii (increasing in magnitude from root toward tip) and increased thickness over the forward 30-percent-chord region. Coordinates of sections parallel to the plane of symmetry are given in table I. The wing was equipped with a leading-edge flap, the chord of which varied from 0 at the root to 25 percent of the wing chord at the tip. The area of the flap was 7 percent of the total wing area. The flap was mounted on the wing by means of brackets which were flush with the lower wing surface. A gap on the upper surface resulted from deflection of the flap about a theoretical hinge line on the lower surface; this gap was filled to provide a smooth upper surface. The fuselage had a Sears-Haack shape of fineness ratio 12.5. Geometry of the model and the equation of the fuselage shape are given in figure 2.

TESTS

Longitudinal force and moment data were obtained for flap deflections of 0°, 4°, 8.5°, 12°, and 16° throughout an angle-of-attack range from -2° to 20°, except at high Mach numbers where the angle limit was reduced because of tunnel power limitations. The major portion of the investigation was made over a Mach number range from 0.25 to 0.92 at a Reynolds number of 3.2×10^6, and over a Reynolds number range from 3.2×10^6 to 15×10^6 at a Mach number of 0.25. In general, the tests at a series of Mach numbers and constant Reynolds number were made with a 0.005-inch wire trip affixed to the upper and lower surfaces of the wing 1/16-inch behind the flap hinge line. The wire was removed for tests at a series of Reynolds numbers and constant Mach number.

The wire was employed to fix transition on the wing in an effort to maintain a skin friction of nearly constant magnitude throughout the angle-of-attack range. The size of the wire was selected on the basis of the empirical results reported in reference 3. To verify that transition was induced by the wire, use was made of a sublimation technique (see ref. 4) employing either acenaphthene or biphenyl in solution with petroleum ether.

Static pressures were measured at the tunnel wall in the region of the model to determine the test conditions for which the data may have been affected by local choking of the air stream at high Mach numbers.

CORRECTIONS

The data have been corrected for tunnel-wall interference associated with lift on the wing, for blockage due to the presence of the tunnel walls, for effects due to a streamwise static-pressure gradient, and for longitudinal force tares of the turntable on which the model was mounted.

The method of reference 5 was used to evaluate the wall interference effects. The resulting corrections which were added to the angles and the coefficients are as follows:

$$\Delta\alpha = 0.607\ C_L$$

$$\Delta C_D = 0.0083\ C_L^{\ 2}$$

$$\Delta C_m = 0.0021\ C_L$$

Corrections to the data to account for the effects of constriction due to the tunnel walls were determined by the method of reference 6. The magnitudes of the corrections to Mach number and dynamic pressure are shown in the following table:

$M_{corrected}$	$M_{uncorrected}$	$\frac{q_{corrected}}{q_{uncorrected}}$
0.25	0.250	1.003
.60	.598	1.005
.80	.794	1.010
.85	.841	1.013
.90	.884	1.019
.92	.900	1.023

A correction was applied to the drag to account for the drag force on the model resulting from the tunnel streamwise static-pressure gradient. The value of this drag coefficient correction was never greater than 0.0006.

The corrections associated with drag tare force due to aerodynamic forces on the exposed surface of the turntable are given in the following table. No attempt has been made to evaluate possible drag forces due to interference between the model and turntable.

M	$C_{D_{tare}}$
0.25	0.0028
.60	.0028
.80	.0032
.85	.0033
.90	.0036
.92	.0038

RESULTS AND DISCUSSION

The basic longitudinal characteristics of the model are presented graphically in figures 3 through 8 for several Reynolds numbers at a Mach number of 0.25, and in figures 9 through 14 for several Mach numbers at a Reynolds number of 3.2×10^6. Selected drag and lift-drag characteristics are presented as functions of Reynolds number in figures 15 and 16 and as functions of Mach number in figures 17 through 20. Figure 21 shows the effect of these parameters on the slopes of the lift and pitching-moment curves. An index to these figures is presented as table II.

Since the Reynolds numbers available at high subsonic speeds for this investigation were low compared with full-scale values, an attempt was made to fix the magnitude of the skin friction throughout the angle-of-attack range by fixing transition near the wing leading edge. Thus, the preponderance of data for the evaluation of the effects of Mach number (figs. 9 through 11) was obtained for the wing with a wire trip affixed to the upper and lower surfaces near the leading edge. Tests were also made with the wire off for flap deflections of 0° and 4° (figs. 12 through 14) in order to evaluate the effects on the aerodynamic characteristics of using the wire to fix transition. A sublimation technique was used in flow studies at high subsonic speeds and showed that with the flap undeflected transition occurred close to the wire, whereas free transition occurred to the rear of the midchord line. However, for most of the low-speed tests the transition wire was not used (see figs. 6 through 8) since sublimation flow studies indicated that the Reynolds numbers available were of sufficient magnitude to cause transition to occur near the leading edge. Tests were also made with the wire on, flap undeflected (figs. 3 through 5), for the purpose of evaluating the effects of Reynolds number on pressure drag for the condition wherein most of the wing was immersed in a turbulent boundary layer. On the basis of sublimation flow studies made at low speeds and low Reynolds numbers, free transition, while not clearly defined, appeared to occur well forward of the midchord position except for a region near the tip; the addition of the wire caused transition to move close to the wire.

At Mach numbers of 0.90 and 0.92, partial choking of the wind tunnel occurred in the region of the model at the higher angles of attack. Dashed lines were used in fairing curves through basic data points for which a state of partial choking of the wind tunnel was indicated.

Drag Characteristics

Effects of Reynolds number.- At low speeds and small flap angles a significant reduction in drag occurred at lift coefficients above 0.2 with increasing Reynolds number from 3.2×10^6 to 15×10^6 (figs. 4(a) and 15). This phenomenon was evidenced at zero flap deflection with and without the transition wire. Up to the lift coefficient at which maximum lift-drag ratio occurred, the reduction in drag coefficient was essentially constant and is attributed to a reduction in skin friction with increasing Reynolds number. This is demonstrated by the data of figure 4(a) and also by figure 16 which shows, for zero flap deflection, the near attainment of the estimated maximum lift-drag ratio throughout the Reynolds number range of the test. Experimental values of minimum drag coefficient for the plane wing-body combination were used for the estimated values of maximum lift-drag ratio, and it was assumed that the span loading was elliptical and the leading-edge suction force was maximum. At higher lift coefficients the drag reductions accompanying an increase in Reynolds number (see fig. 15) are attributed to a greater effective leading-edge suction force. Apparently the low pressures required for attainment of full effective leading-edge suction force are not realized at low Reynolds numbers with the flap at zero deflection. However, as indicated in figure 15, there is (at low Reynolds number) a progressive decrease in drag coefficient at constant lift coefficient with increasing flap deflection, and the effects of Reynolds number practically disappear. It is surmised that the camber introduced by deflection of the flap redistributes the suction pressures over a larger region. Thus the magnitude of the pressures for full leading-edge suction (i.e., pressures required for minimum drag due to lift) would be lower than if they were concentrated at the leading edge, and therefore these pressures are more nearly physically attainable.

At Mach numbers of 0.60 and 0.80 there was little effect of Reynolds number on the drag of the model with the flap undeflected (figs. 4(b), 5(b), and 15). Although the range of test Reynolds numbers was rather small at these speeds, it encompassed a region wherein large drag reductions occurred at low speeds. The effect of Reynolds number on the drag of the model with flap deflected would be expected to be small on the basis of the low-speed data. This thesis agrees with the results shown in reference 7, wherein data at transonic speeds in a range of Reynolds numbers from 2×10^6 to 6×10^6 are presented for a thin wing of somewhat similar plan form, having an NACA 6A series section and 6° nose droop.

Effects of Mach number.- Inasmuch as there were large Reynolds number effects on drag at low speeds, only the data at a Reynolds number of 15×10^6 will be used in discussion of the low-speed data as they relate to the effects of Mach number. As shown in figures 7(e) and 15, deflecting the flap to 16° resulted in a slight increase in zero-lift drag coefficient, but the drag variation with lift was not altered up to a lift coefficient of 0.55. Above this value substantial reductions in drag, and therefore increase in lift-drag ratio (fig. 8(c)), occurred with increasing flap deflection. The ineffectiveness of the flap in reducing the drag coefficient at lift coefficients below 0.55 is probably indicative that the drag due to lift for the plane wing was near the theoretical minimum, which corresponds to elliptical span loading and full leading-edge suction. This was the case at lift coefficients of the order of 0.3, as is shown by the comparison in figure 16 of experimental and estimated maximum lift-drag ratios.

At Mach numbers of 0.60 and above, the drag characteristics associated with flap deflection differed considerably from those at low speeds and at high Reynolds numbers. As seen in figure 17, deflecting the flap caused a penalty in zero-lift drag coefficient which increased with increasing flap angle. It may be noted that the drag increment due to 4° flap deflection was much greater for the model having no wire trip than for the model with the wire trip. This is not surprising in view of the results of flow studies which showed that while transition was induced close to the wire, deflection of the flap in itself caused transition to move well forward from its location on the rear portion of the wing with the flap in the undeflected position. Deflection of the flap at lift coefficients of 0.2 and greater resulted in drag reductions which generally diminished with increasing Mach number above a Mach number of 0.80. It is evident that at lift coefficients of 0.2 and 0.4 the larger flap deflections (excluding 16°) provided the greatest drag reductions between Mach numbers of 0.60 and 0.85, whereas at higher speeds maximum reductions were achieved with 4° flap deflection. At still higher lift coefficients, the larger flap angles provided the greatest drag reductions even at a Mach number of 0.90.

The degree to which the flap was effective in achieving the estimated maximum lift-drag ratio is shown in figure 18. As noted earlier, the estimated maximum lift-drag ratios were based on the experimental minimum drag for the plane wing-body combination (transition wire on) and on the assumptions of elliptical span loading and full leading-edge suction. At a Mach number of 0.60, the estimated value was fully attained with a flap angle of 12°, compared to about 85 percent of the estimated value for the plane wing. At a Mach number of 0.90, about 95 percent of the estimated value was attained with a flap angle of 4° compared to about 80 percent for the plane wing. These improvements are further exemplified in figure 19, which shows the effect of Mach number on the ratio of lift-drag ratio of the wing with flap deflected to that of the plane wing. Envelopes of these curves are shown in figure 20, in which is also presented the ratio of lift-drag ratio of the conically cambered wings of reference 2

to that of the plane wing of the same reference, both wings having surface roughness strips at the same location as the transition wires employed herein. It is apparent that in the Mach number range from 0.60 to 0.92 slightly greater improvement in maximum lift-drag ratio was achieved through optimum leading-edge flap deflection than through conical camber. For example, at a Mach number of 0.90 the increase in maximum lift-drag ratio due to flap deflection ($\delta = 4^{\circ}$) was about 16 percent compared to about 10 percent due to conical camber ($C_{L_d} = 0.22$). At lift coefficients greater than those for which maximum lift-drag ratio occurred (see curves for $C_L = 0.4$ and 0.6), the flap provided larger increases in lift-drag ratio than did conical camber below a Mach number of 0.80; whereas, conical camber was more advantageous at speeds near a Mach number of 0.90.

Lift and Pitching-Moment Characteristics

Examination of the low-speed lift and pitching-moment data in figure 6 and of the high-speed data in figure 9 reveals that, in general, deflection of the flap resulted in more nearly linear pitching-moment curves. It may be further noted that only a slight negative moment shift occurred with flap deflection; consequently, the drag associated with trimming these moments would be small. The data in figure 21 show that throughout the Reynolds number and Mach number range of the investigation the slopes of the lift and moment curves near zero lift generally increased slightly with increasing flap deflection.

CONCLUSIONS

An experimental investigation has been conducted to determine the effectiveness of an inverse-taper leading-edge flap in improving primarily the drag characteristics at high subsonic speeds of a wing-body combination having an aspect ratio of 3 and 45° of leading-edge sweepback. The results can be summarized as follows:

1. In the range of Mach numbers from 0.60 to 0.92, deflection of the flap resulted in significant reductions in drag at lift coefficients of 0.2 and greater. The maximum lift-drag ratios were nearly 20 percent higher than those of the plane wing and were near the estimated maximums, based on the assumptions of elliptic span loading and full leading-edge suction.

2. Compared to conical camber, the leading-edge flap promoted slightly larger gains in maximum lift-drag ratio in the Mach number range from 0.60 to 0.92.

3. At low speeds and at a Reynolds number of 15 million the flap was effective in reducing drag coefficient only at lift coefficients above 0.55.

4. In general, deflecting the flap resulted in little change in lift and static stability.

Ames Aeronautical Laboratory
National Advisory Committee for Aeronautics
Moffett Field, Calif., May 13, 1958

REFERENCES

1. Hall, Charles F.: Lift, Drag, and Pitching Moment of Low-Aspect-Ratio Wings at Subsonic and Supersonic Speeds. NACA RM A53A30, 1953.

2. Sammonds, Robert I., and Reynolds, Robert M.: The Effect of Conical Camber on the Static Longitudinal, Lateral, and Directional Characteristics of a 45° Sweptback Wing at Mach Numbers Up to 0.96. NACA RM A56D02, 1956.

3. Winter, K. G., Scott-Wilson, J. B., and Davies, F. V.: Methods of Determination and of Fixing Boundary-Layer Transition on Wind Tunnel Models at Supersonic Speeds. R.A.E. TN Aero. 2341, (British), 1954. (Also available as A.R.C. rep. 17,416, C.P. 212, 1955, and AGARD rep. AG 17/p7, 1954, pp. 167-191)

4. Main-Smith, J. D.: Chemical Solids as Diffusable Coating Films for Visual Indications of Boundary-Layer Transition in Air and Water. R. & M. No. 2755 (13115), British A.R.C., 1954. (Also published as R.A.E. Chem. 466, Feb. 1950)

5. Sivells, James C., and Salmi, Rachel M.: Jet-Boundary Corrections for Complete and Semispan Swept Wings in Closed Circular Wind Tunnels. NACA TN 2454, 1951.

6. Herriot, John G.: Blockage Corrections for Three-Dimensional-Flow Closed-Throat Wind Tunnels, With Consideration of the Effect of Compressibility. NACA Rep. 995, 1950. (Supersedes NACA RM A7B28)

7. Schmeer, James W., and Cooper, J. Lawrence: Effects of Increasing Reynolds Number From 2×10^6 to 6×10^6 on the Aerodynamic Characteristics at Transonic Speeds of a 45° Swept Wing With 6° Leading-Edge Droop. NACA RM L54L10, 1955.

TABLE I.- COORDINATES OF AIRFOIL SECTIONS FOR PLANE WING

[Coordinates are presented for sections parallel to the plane of symmetry]

2y/b	x percent c	z percent c	x percent c	z percent c	2y/b	x percent c	z percent c	x percent c	z percent c
0[a]	0	0	47.325	2.522	0.67[d]	0	0	47.325	2.522
	.672	.464	52.440	2.438		.672	.745	52.440	2.438
	1.008	.559	57.404	2.304		1.008	.842	57.404	2.304
	1.678	.704	62.223	2.132		1.678	.972	62.223	2.132
	3.340	.964	66.903	1.931		3.340	1.242	66.903	1.931
	6.623	1.317	71.452	1.709		6.623	1.609	71.452	1.709
	9.850	1.571	75.872	1.468		9.850	1.847	75.872	1.468
	13.023	1.776	80.170	1.217		13.023	2.030	80.170	1.217
	19.213	2.077	84.352	.963		19.213	2.236	84.352	.963
	25.200	2.289	88.421	.715		25.200	2.354	88.421	.715
	30.997	2.429	92.384	.473		30.997	2.429	92.384	.473
	36.610	2.511	96.212	.238		36.610	2.511	96.212	.238
	42.050	2.541	100.000	.009		42.050	2.541	100.000	.009
0.25[b]	0	0	47.325	2.522	0.83[e]	0	0	47.325	2.522
	.672	.572	52.440	2.438		.672	.817	52.440	2.438
	1.008	.663	57.404	2.304		1.008	.920	57.404	2.304
	1.678	.808	62.223	2.132		1.678	1.050	62.223	2.132
	3.340	1.067	66.903	1.931		3.340	1.322	66.903	1.931
	6.623	1.426	71.452	1.709		6.623	1.685	71.452	1.709
	9.850	1.677	75.872	1.468		9.850	1.931	75.872	1.468
	13.023	1.868	80.170	1.217		13.023	2.100	80.170	1.217
	19.213	2.135	84.352	.963		19.213	2.281	84.352	.963
	25.200	2.310	88.421	.715		25.200	2.372	88.421	.715
	30.997	2.429	92.384	.473		30.997	2.429	92.384	.473
	36.610	2.511	96.212	.238		36.610	2.511	96.212	.238
	42.050	2.541	100.000	.009		42.050	2.541	100.000	.009
0.50[c]	0	0	47.325	2.522	1.00[f]	0	0	47.325	2.522
	.672	.676	52.440	2.438		.672	.891	52.440	2.438
	1.008	.768	57.404	2.304		1.008	.988	57.404	2.304
	1.678	.907	62.223	2.132		1.678	1.118	62.223	2.132
	3.340	1.176	66.903	1.931		3.340	1.393	66.903	1.931
	6.623	1.528	71.452	1.709		6.623	1.750	71.452	1.709
	9.850	1.778	75.872	1.468		9.850	1.993	75.872	1.468
	13.023	1.963	80.170	1.217		13.023	2.155	80.170	1.217
	19.213	2.194	84.352	.963		19.213	2.317	84.352	.963
	25.200	2.333	88.421	.715		25.200	2.382	88.421	.715
	30.997	2.429	92.384	.473		30.997	2.429	92.384	.473
	36.610	2.511	96.212	.238		36.610	2.511	96.212	.238
	42.050	2.541	100.000	.009		42.050	2.541	100.000	.009

[a]Leading-edge radius: 0.190 percent chord
[b]Leading-edge radius: 0.236 percent chord
[c]Leading-edge radius: 0.370 percent chord
[d]Leading-edge radius: 0.520 percent chord
[e]Leading-edge radius: 0.713 percent chord
[f]Leading-edge radius: 0.924 percent chord

TABLE II.- INDEX OF DATA FIGURES

Figure	Variables	M	$R \times 10^{-6}$	δ	Transition wire
3	C_m, α vs. C_L	0.25 to 0.80	3.2 to 15.0	0	On
4	C_D vs. C_L	0.25 to 0.80	3.2 to 15.0	0	On
5	$\frac{L}{D}$ vs. C_L	0.25 to 0.80	3.2 to 15.0	0	On
6	C_m, α vs. C_L	0.25	3.2 to 15.0	0 to 16	Off
7	C_D vs. C_L	0.25	3.2 to 15.0	0 to 16	Off
8	$\frac{L}{D}$ vs. C_L	0.25	3.2 to 15.0	0 to 16	Off
9	C_m, α vs. C_L	0.25 to 0.92	3.2	0 to 16	On
10	C_D vs. C_L	0.60 to 0.92	3.2	0 to 16	On
11	$\frac{L}{D}$ vs. C_L	0.60 to 0.92	3.2	0 to 16	On
12	C_m, α vs. C_L	0.60 to 0.92	3.2	0, 4	Off
13	C_D vs. C_L	0.60 to 0.92	3.2	0, 4	Off
14	$\frac{L}{D}$ vs. C_L	0.60 to 0.92	3.2	0, 4	Off
15	C_D vs. R	0.25 to 0.80	3.2 to 15.0	0 to 16	On and off
16	$\left(\frac{L}{D}\right)_{max}$, $C_{L_{\left(\frac{L}{D}\right)_{max}}}$ vs. R	0.25	3.2 to 15.0	0 to 16	Off
17	C_D vs. M	0.60 to 0.92	3.2	0 to 16	On and off
18	$\left(\frac{L}{D}\right)_{max}$, $C_{L_{\left(\frac{L}{D}\right)_{max}}}$ vs. M	0.60 to 0.92	3.2	0 to 16	On
19	$\frac{L/D}{(L/D)_{\delta=0}}$ vs. M	0.60 to 0.92	3.2	0 to 16	On
20	$\frac{L/D}{(L/D)_{\delta=0}}$ vs. M	0.60 to 0.92	3.2	Optimum	On
21	$\frac{dC_L}{d\alpha}$, $\frac{dC_m}{dC_L}$ vs. M, R	0.25 to 0.92	3.2 to 15.0	0 to 16	On and off

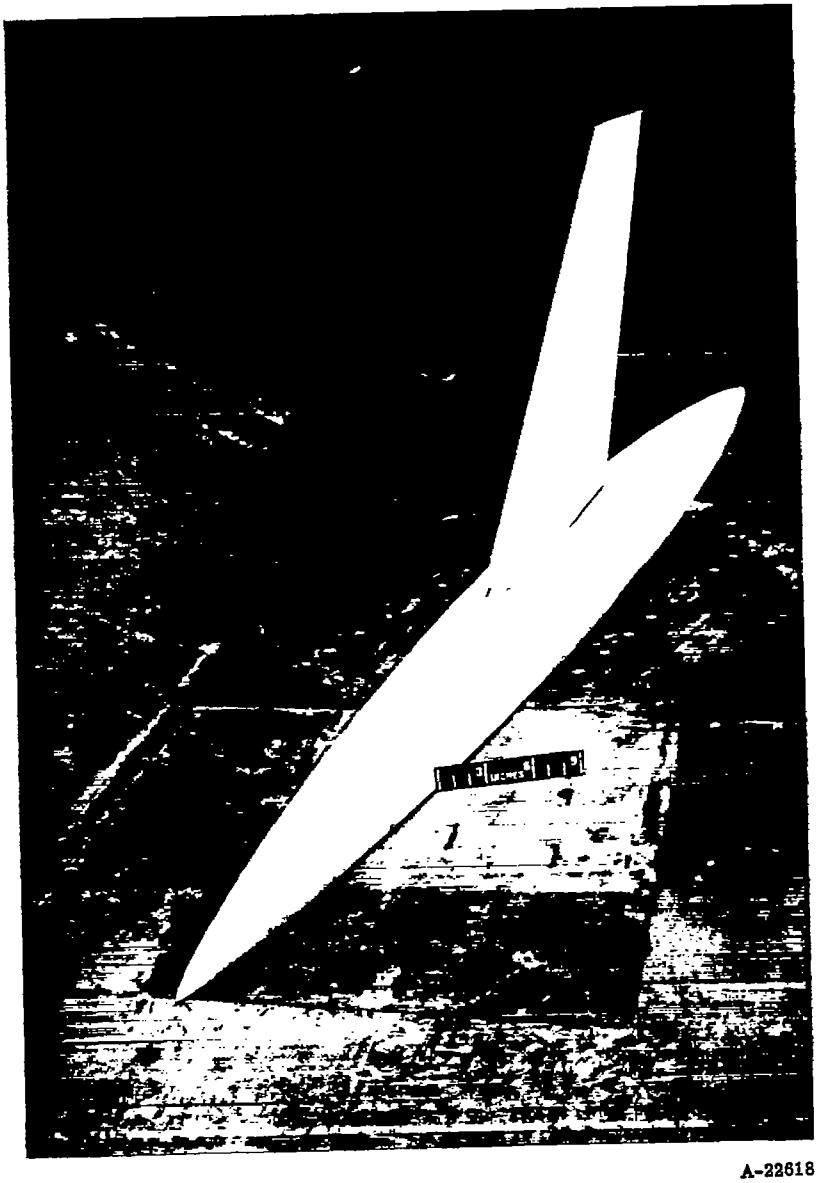

A-22618

Figure 1.- Photograph of the model mounted in the wind tunnel.

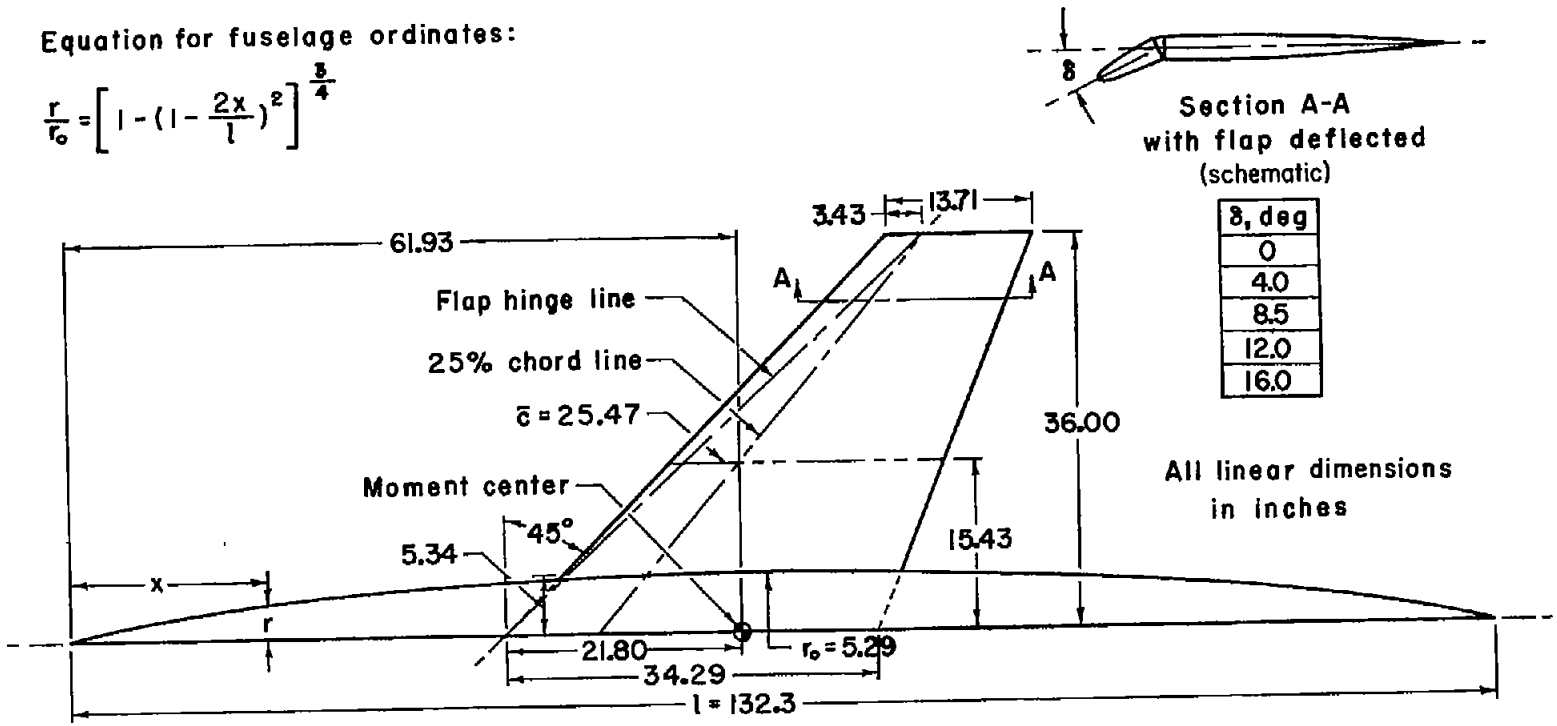

Figure 2.- Geometric characteristics of the model.

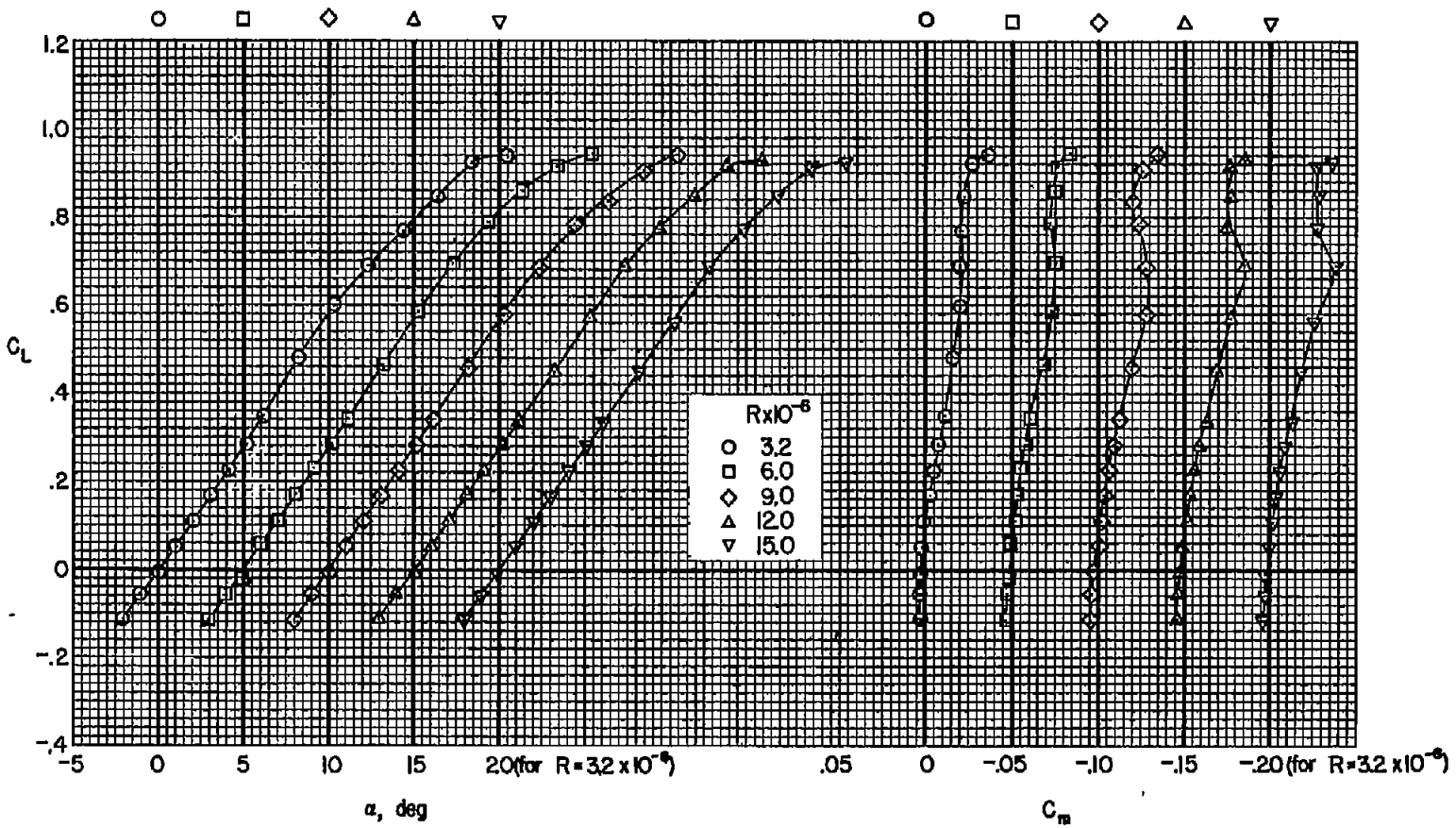

(a) M = 0.25

Figure 3.- The effect of Reynolds number on the lift and pitching-moment coefficient of the model; wire on, $\delta = 0^{\circ}$.

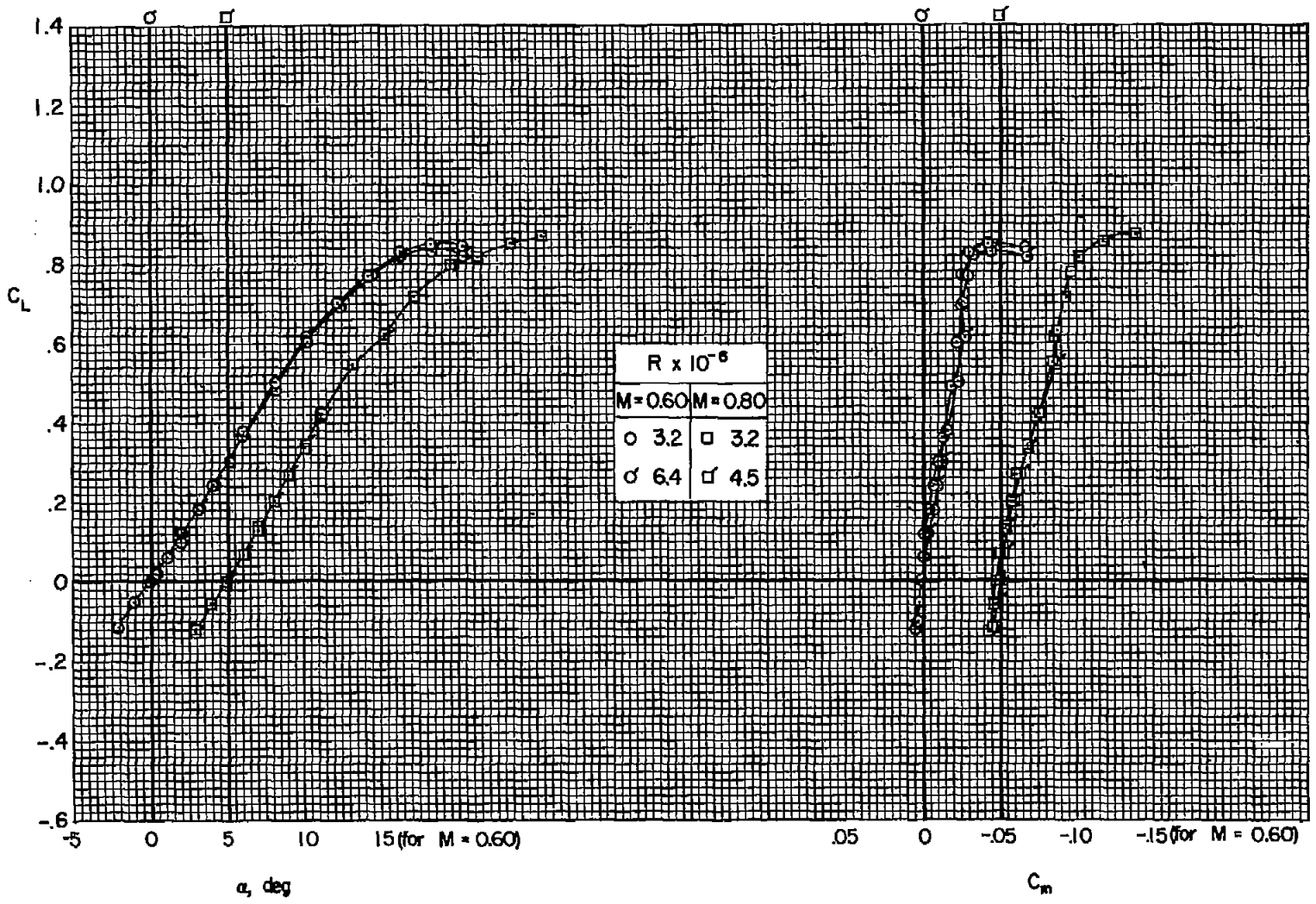

(b) M = 0.60, 0.80

Figure 3.- Concluded.

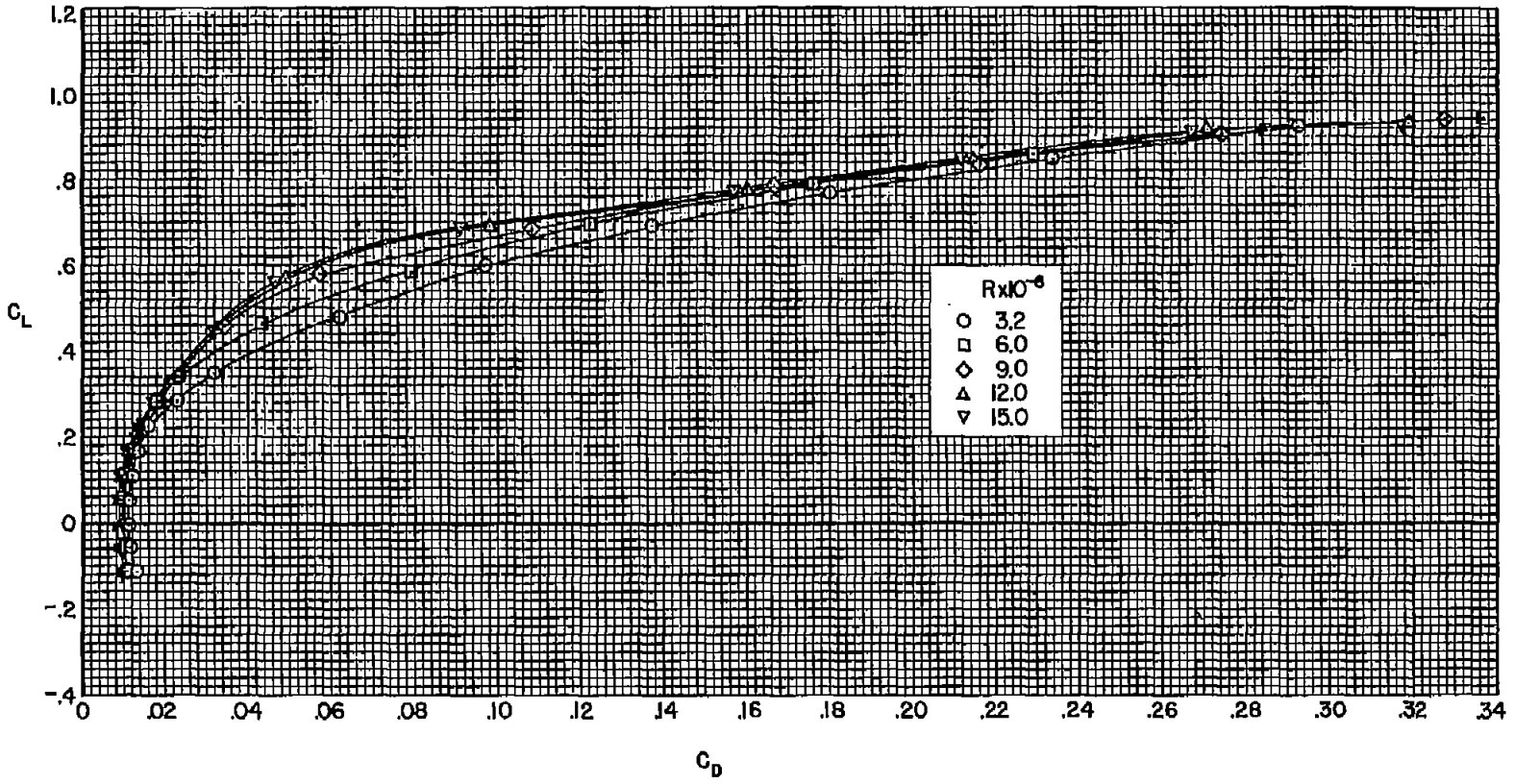

(a) M = 0.25

Figure 4.- The effect of Reynolds number on the drag coefficients of the model; wire on, $\delta = 0^{\circ}$.

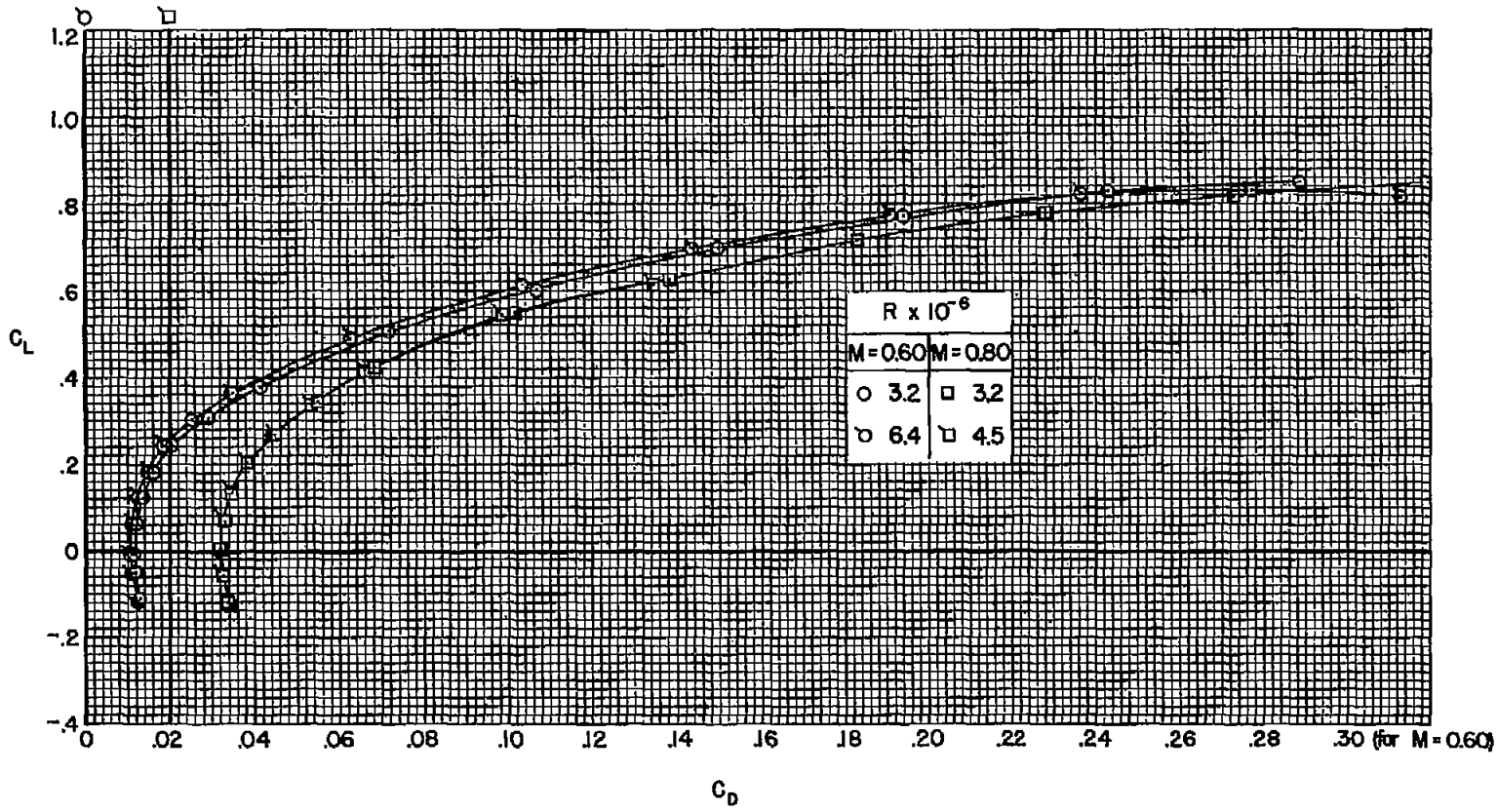

(b) M = 0.60, 0.80

Figure 4.- Concluded.

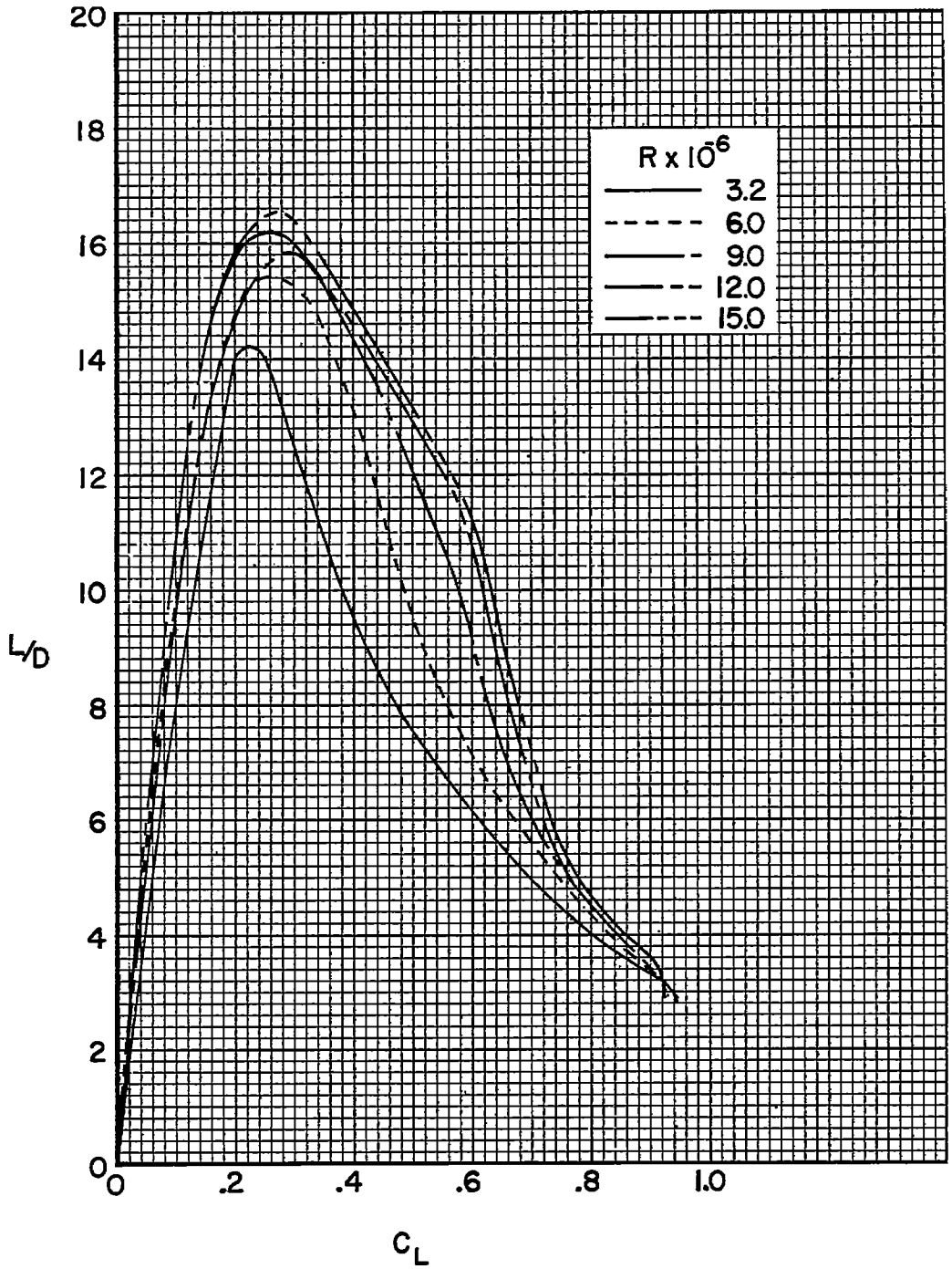

(a) M = 0.25

Figure 5.- The effect of Reynolds number on the lift-drag ratios of the model; wire on, $\delta = 0^{\circ}$.

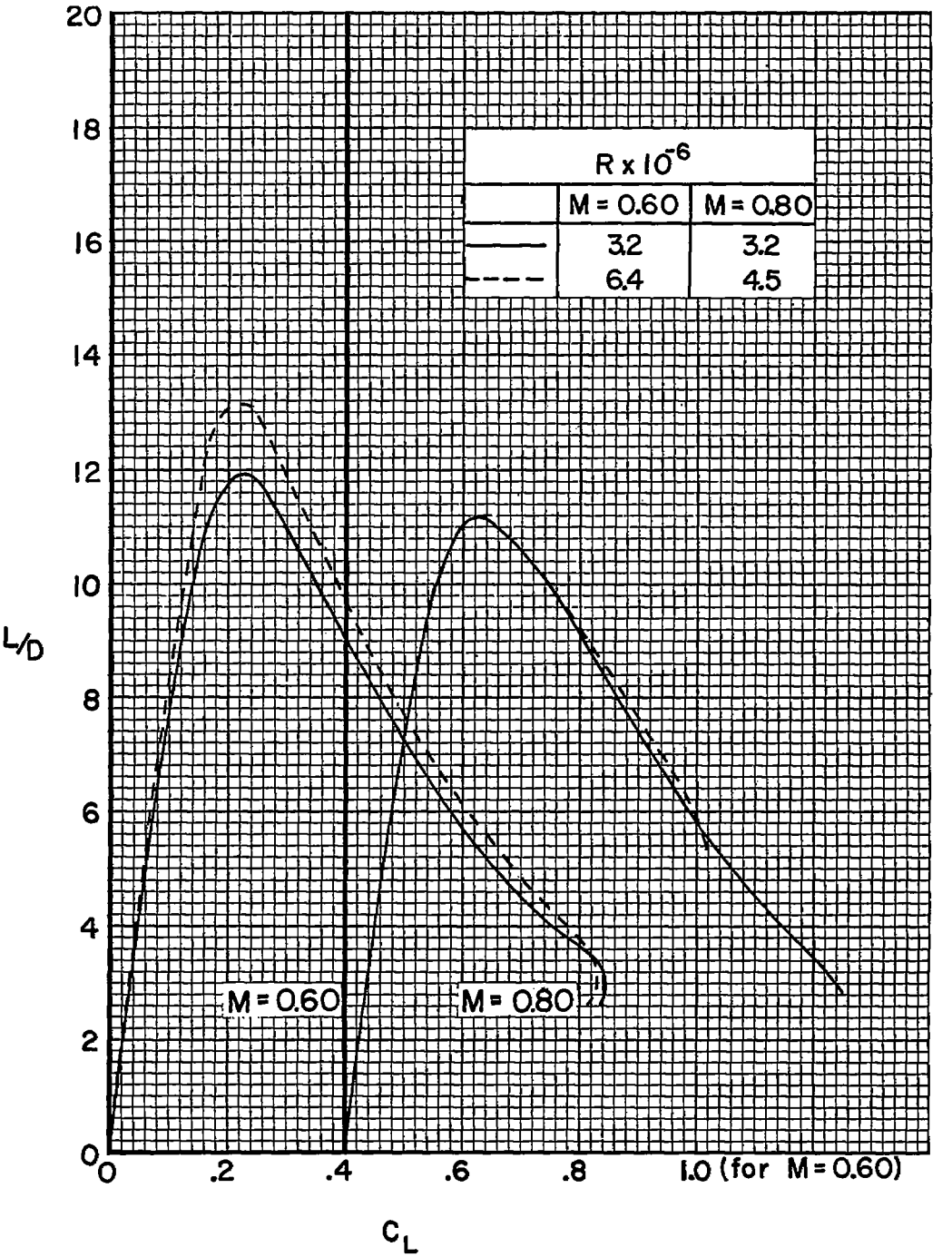

(b) M = 0.60, 0.80

Figure 5.- Concluded.

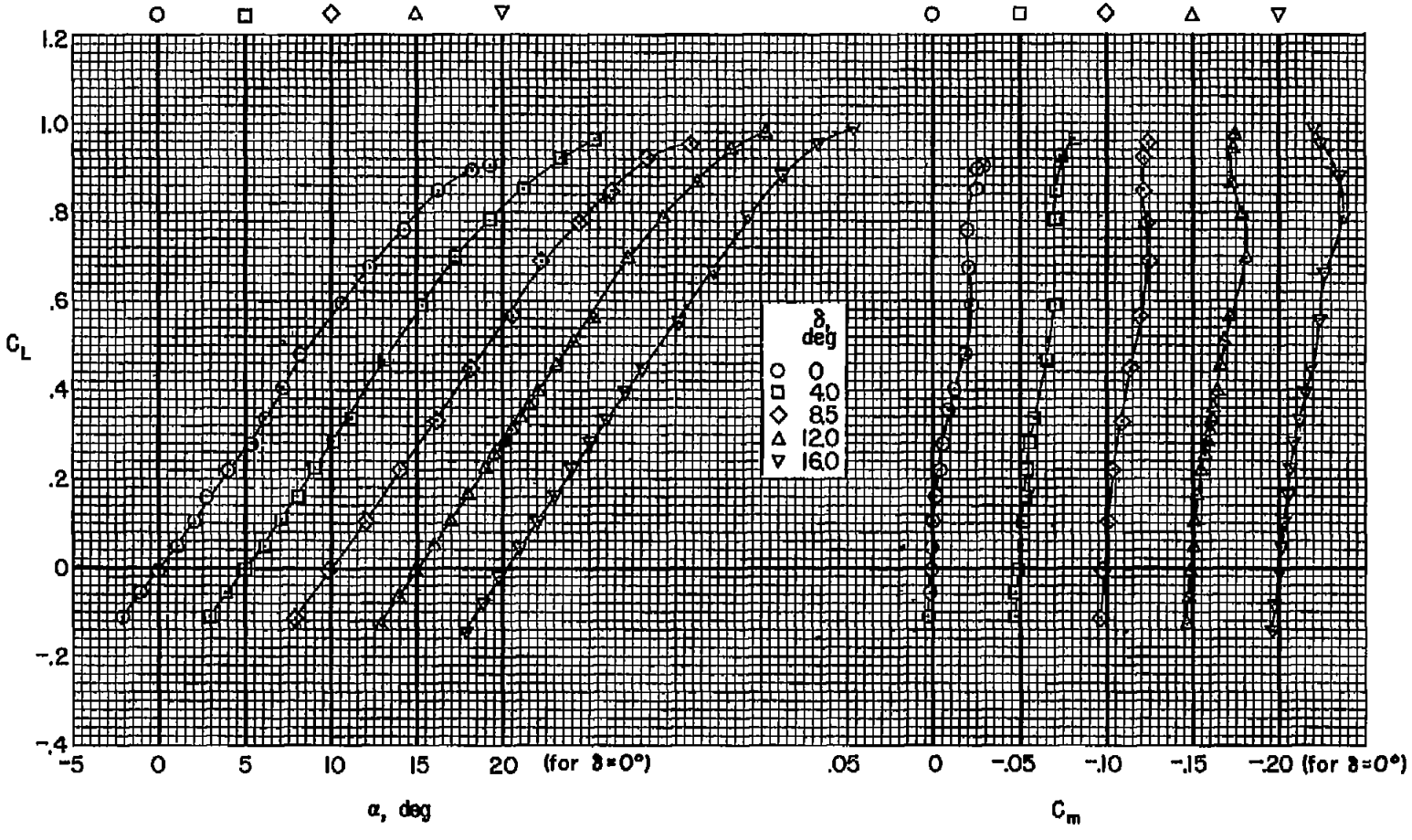

(a) R = 3.2×10^6

Figure 6.- The effect of flap deflection on the lift and pitching-moment coefficients of the model; wire off, M = 0.25.

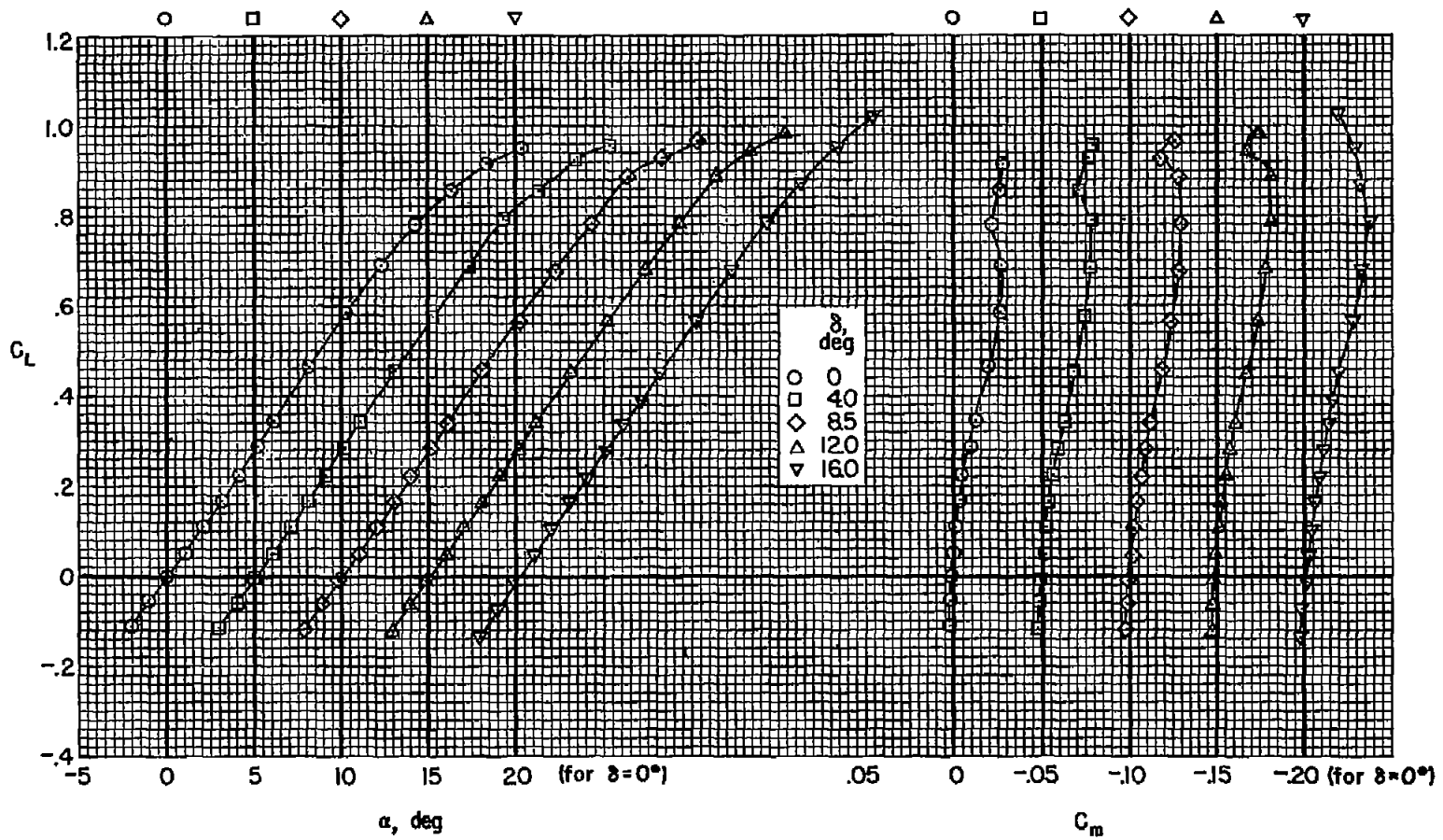

(b) R = 6×10^6

Figure 6.- Continued.

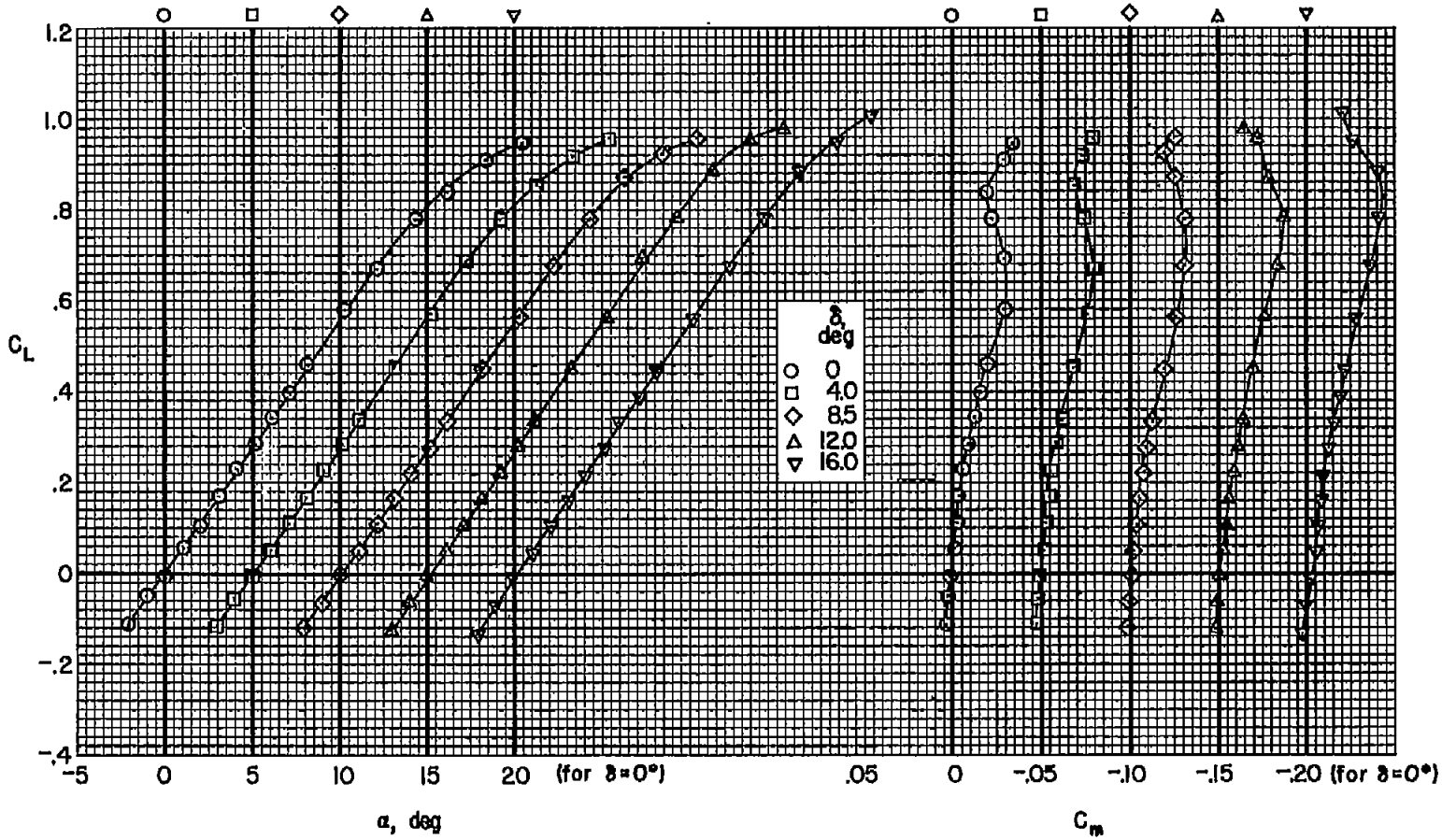

(c) R = 9×10^6

Figure 6.- Continued.

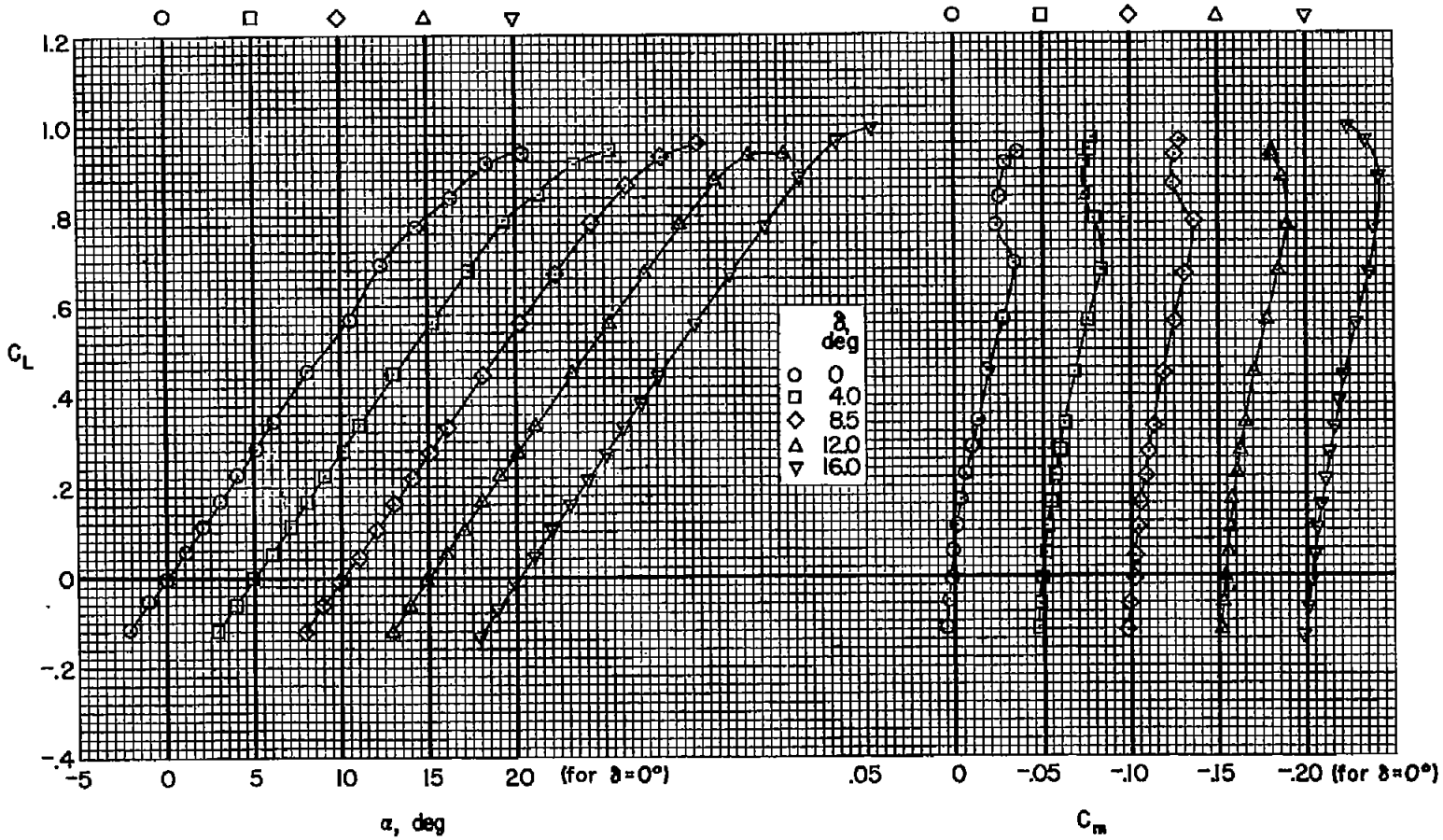

(d) R = 12×10^6

Figure 6.- Continued.

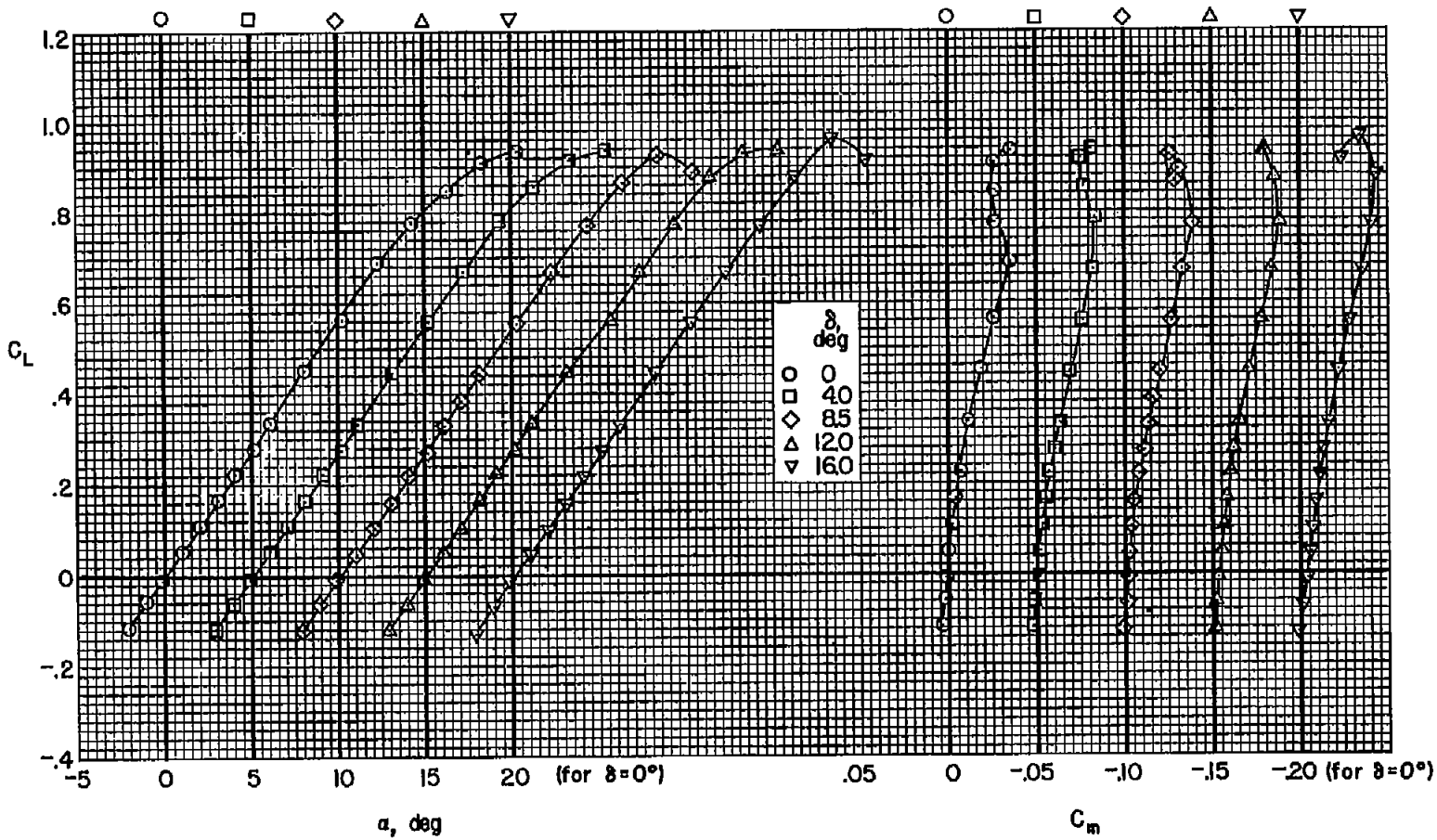

(e) R = 15×10^6

Figure 6.- Concluded.

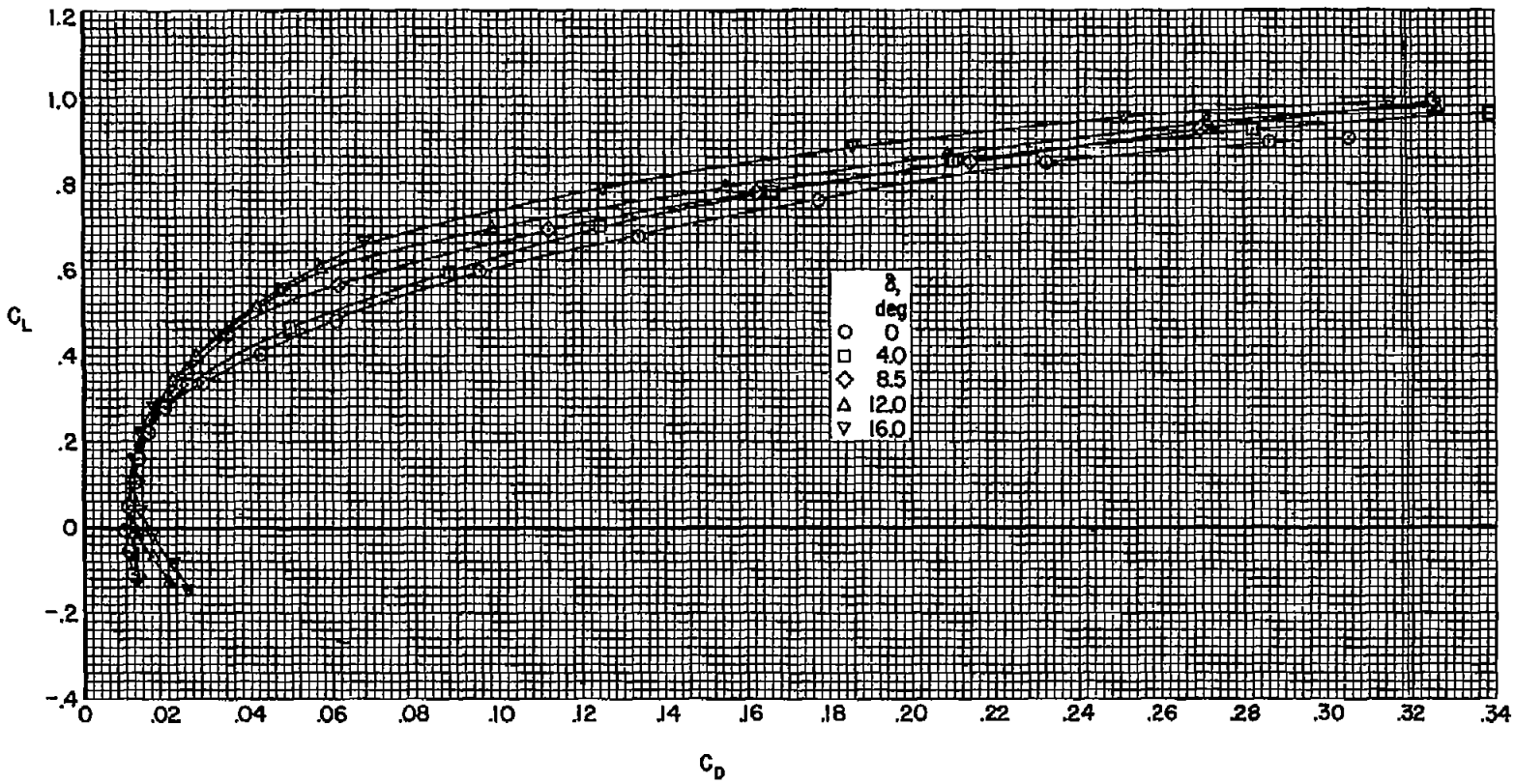

(a) R = 3.2×10^6

Figure 7.- The effect of flap deflection on the drag coefficients of the model; wire off, M = 0.25.

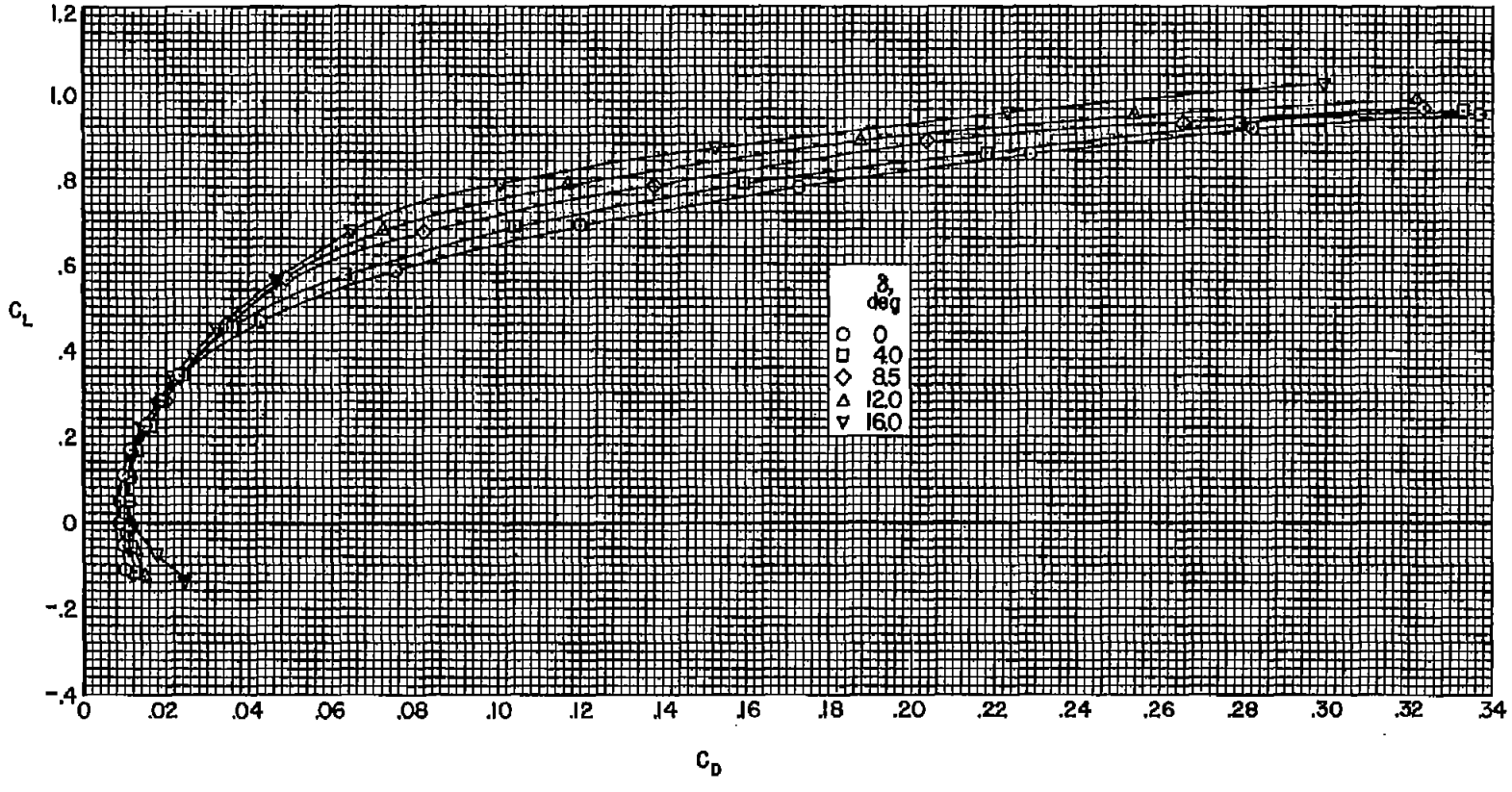

(b) R = 6×10^6

Figure 7.- Continued.

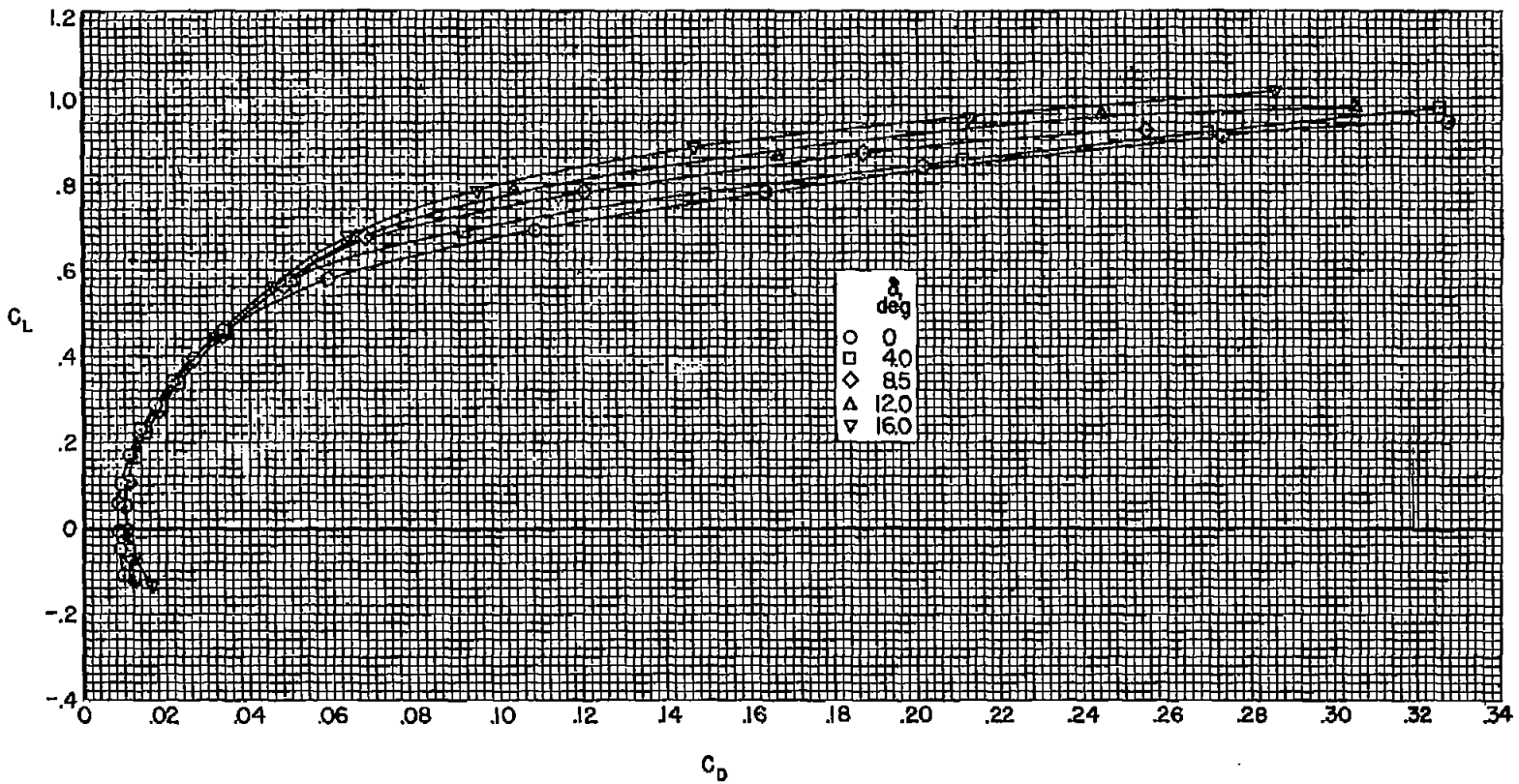

(c) R = 9×10^6

Figure 7.- Continued.

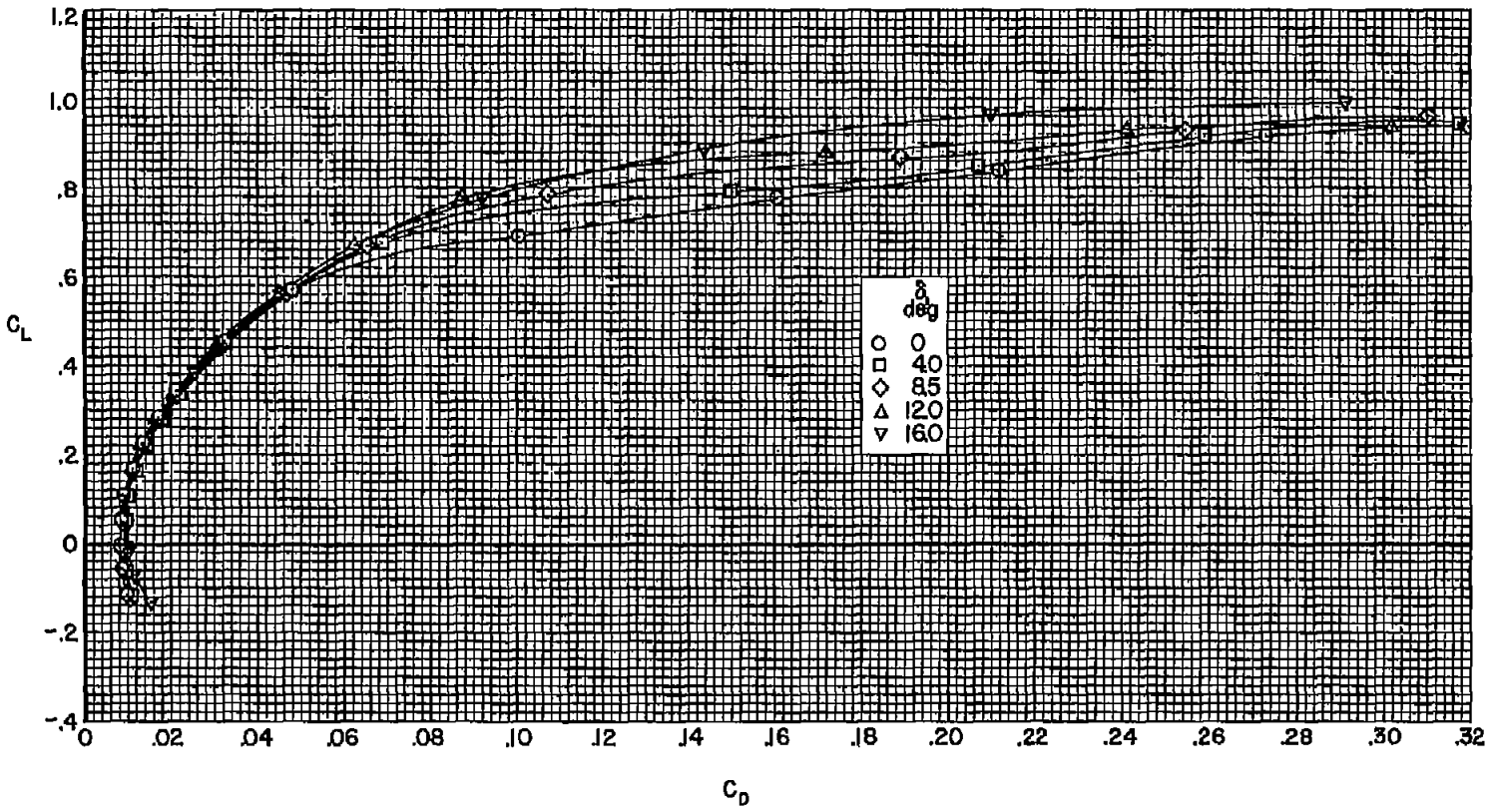

(d) R = 12×10^6

Figure 7.- Continued.

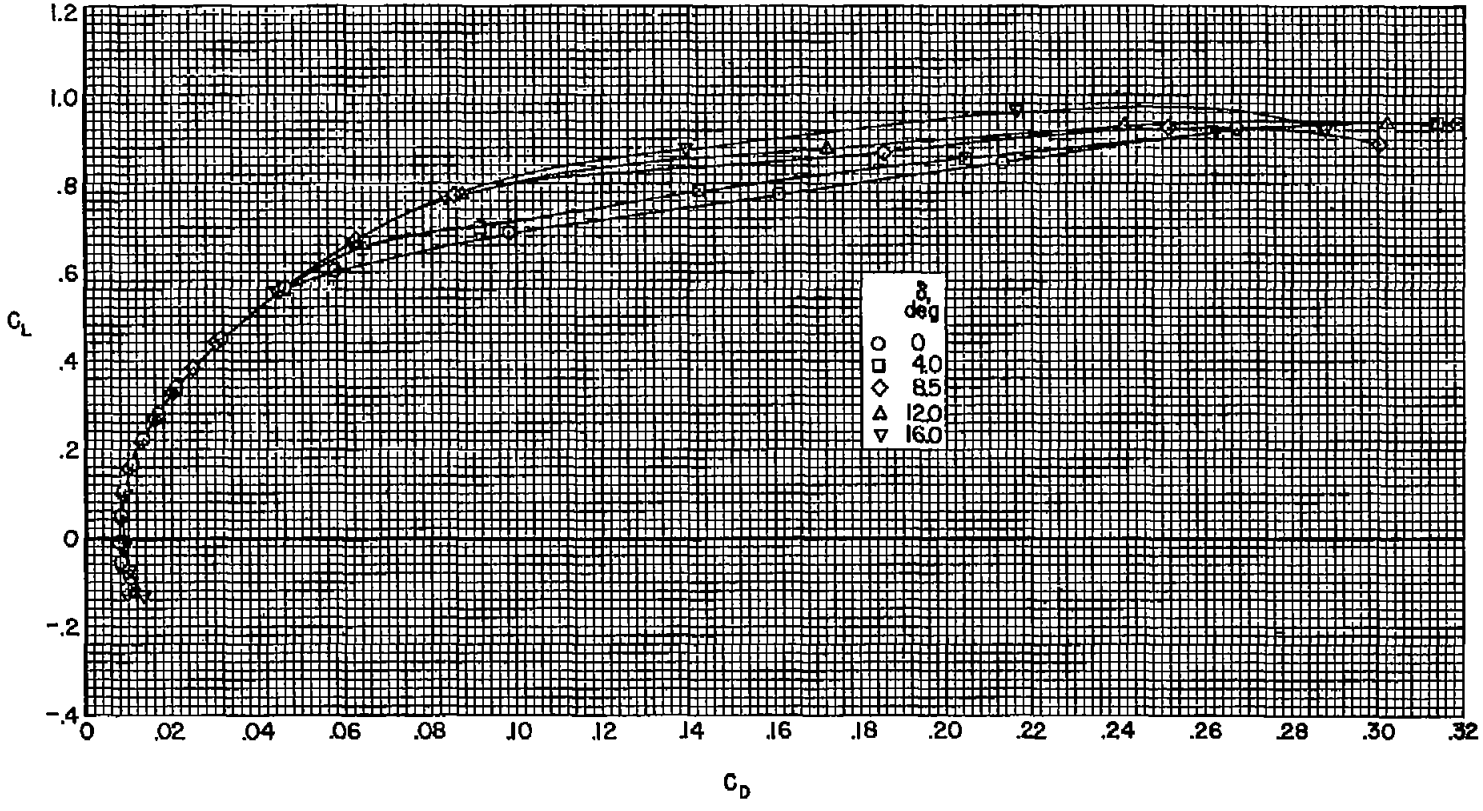

(e) R = 15×10^6

Figure 7.- Concluded.

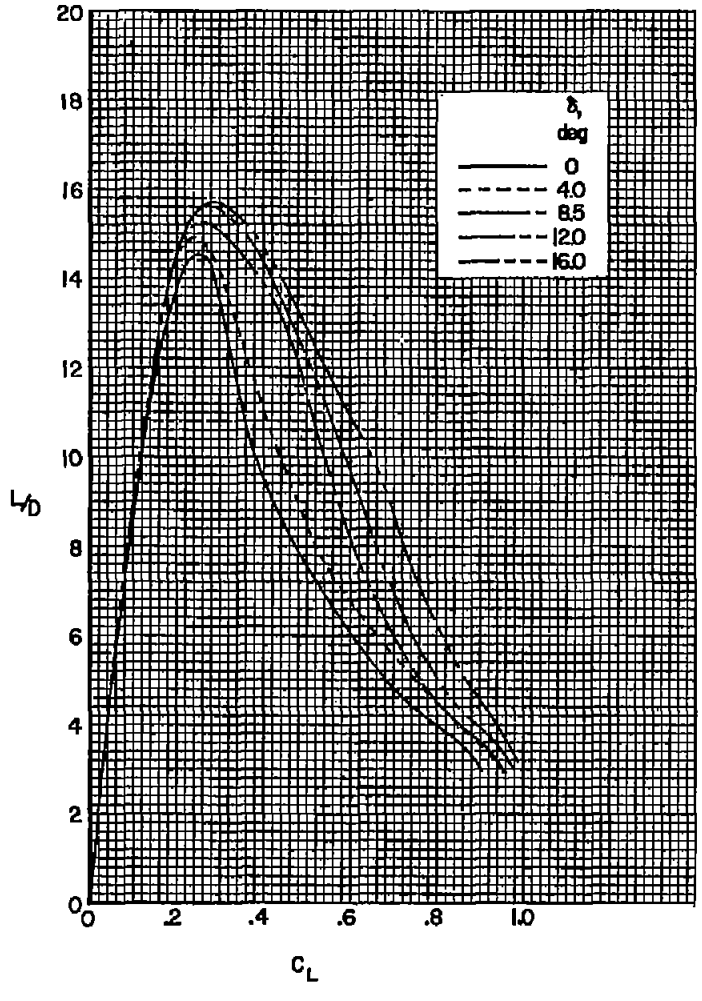

(a) R = 3.2×10^6

Figure 8.- The effect of flap deflection on the lift-drag ratios of the model; wire off, M = 0.25.

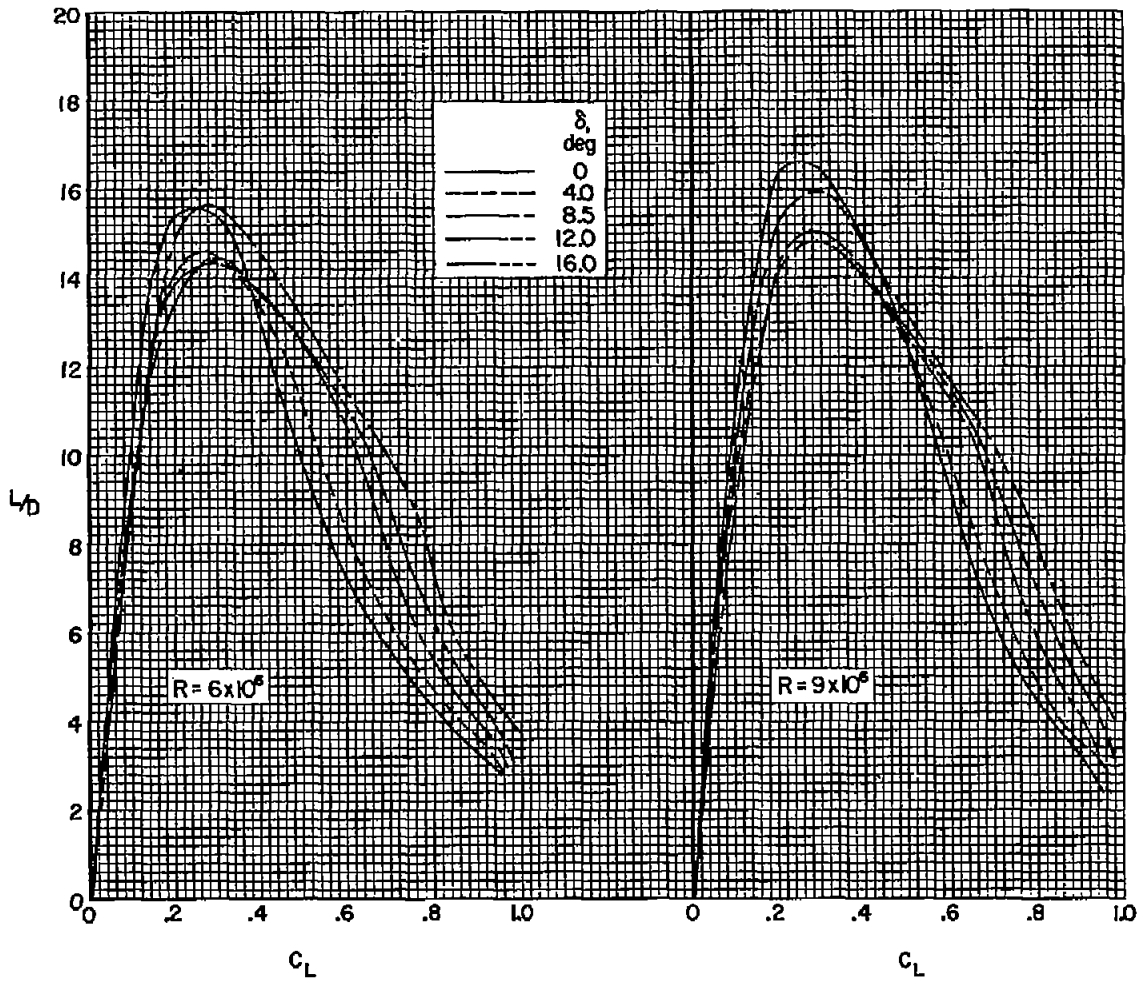

(b) R = 6 and 9×10^6

Figure 8.- Continued.

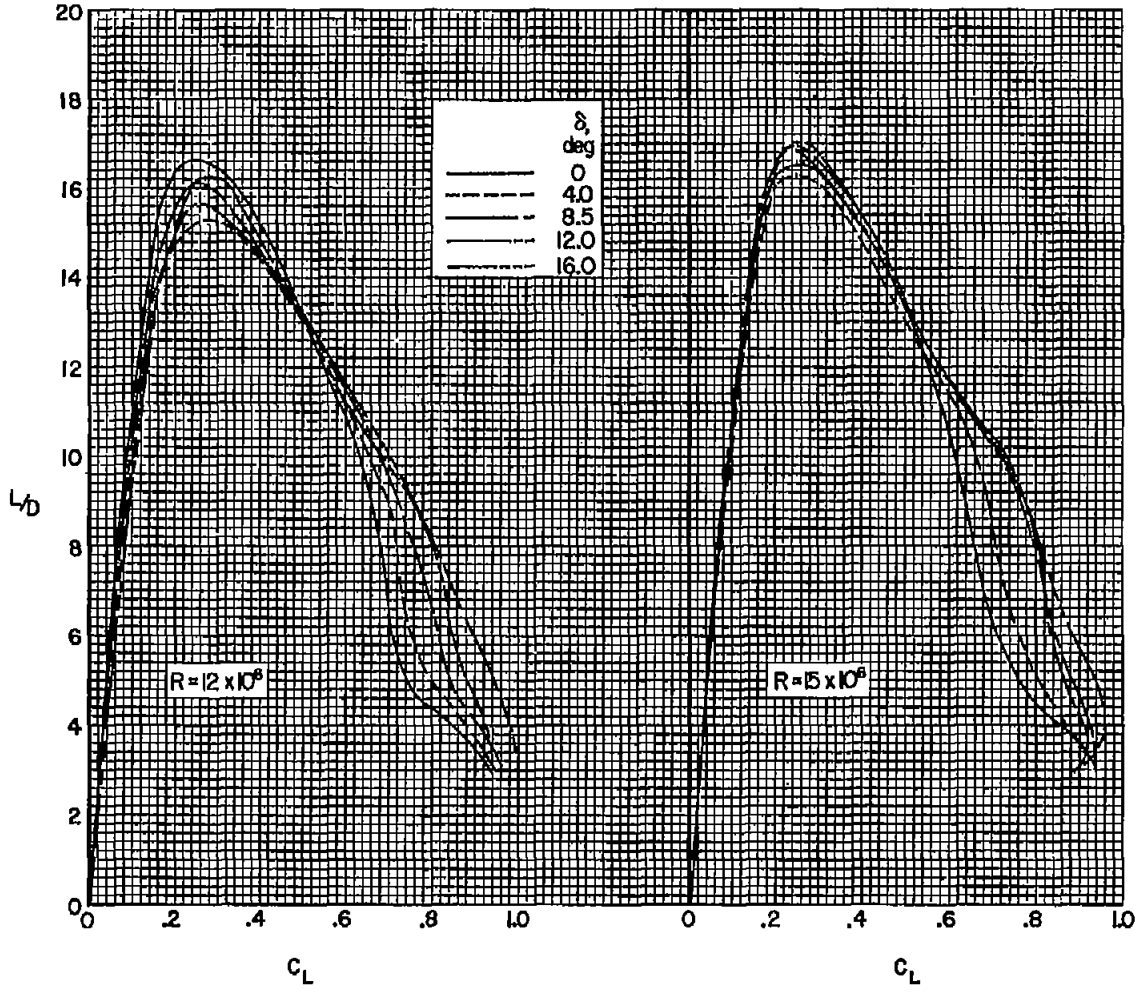

(c) R = 12 and 15×10^6

Figure 8.- Concluded.

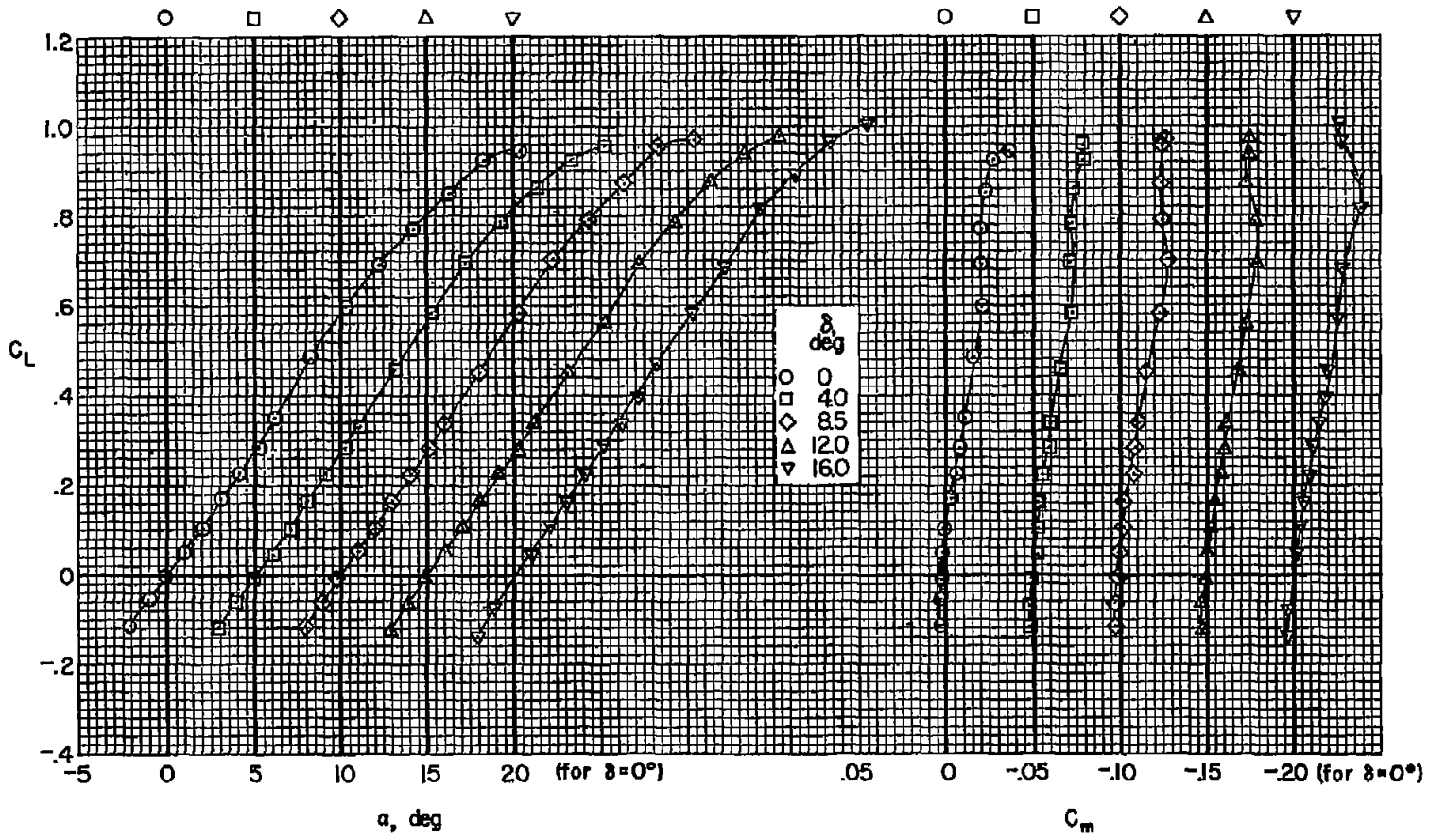

(a) M = 0.25

Figure 9.- The effect of flap deflection on the lift and pitching-moment coefficients of the model; wire on, R = 3.2×10^6.

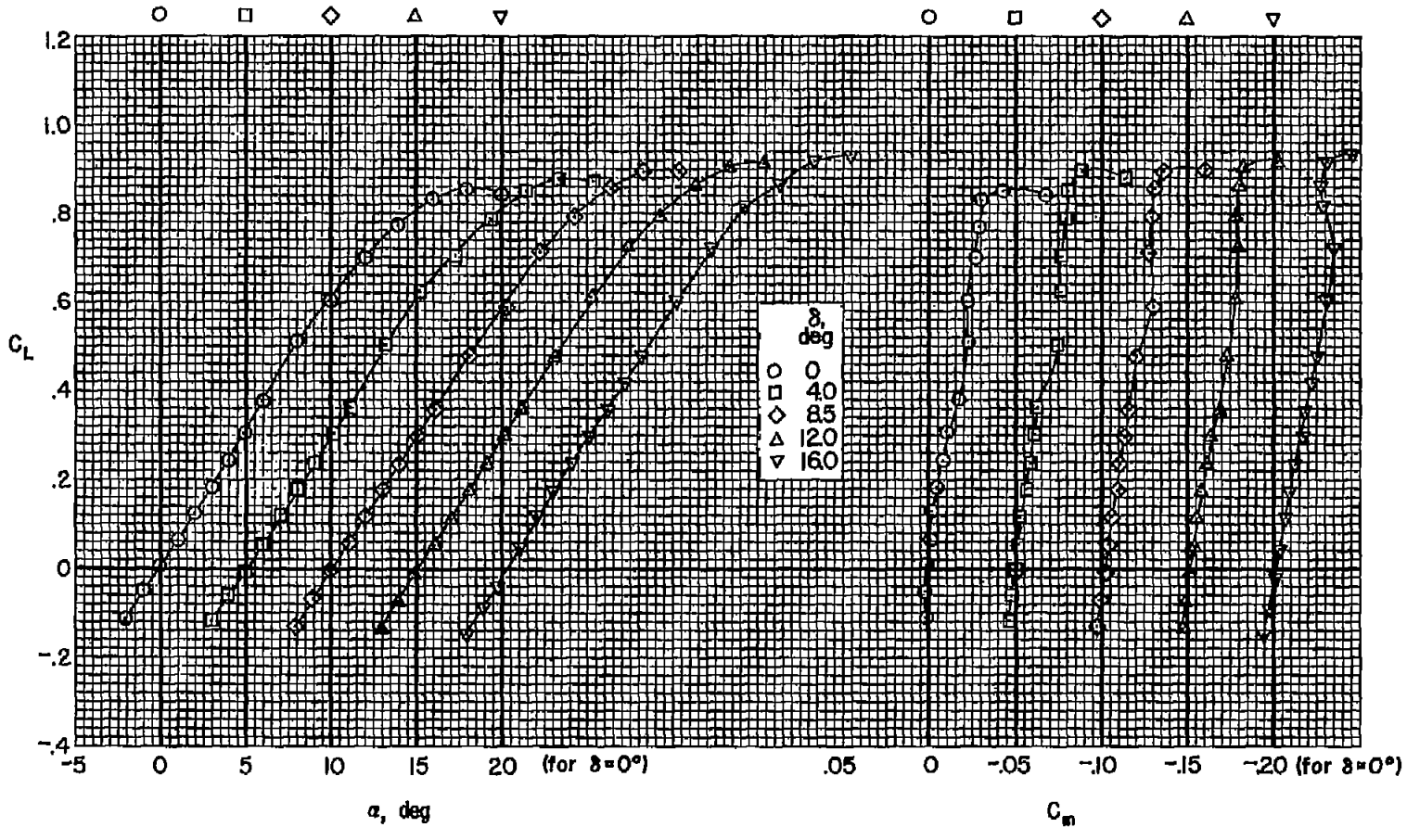

(b) M = 0.60

Figure 9.- Continued.

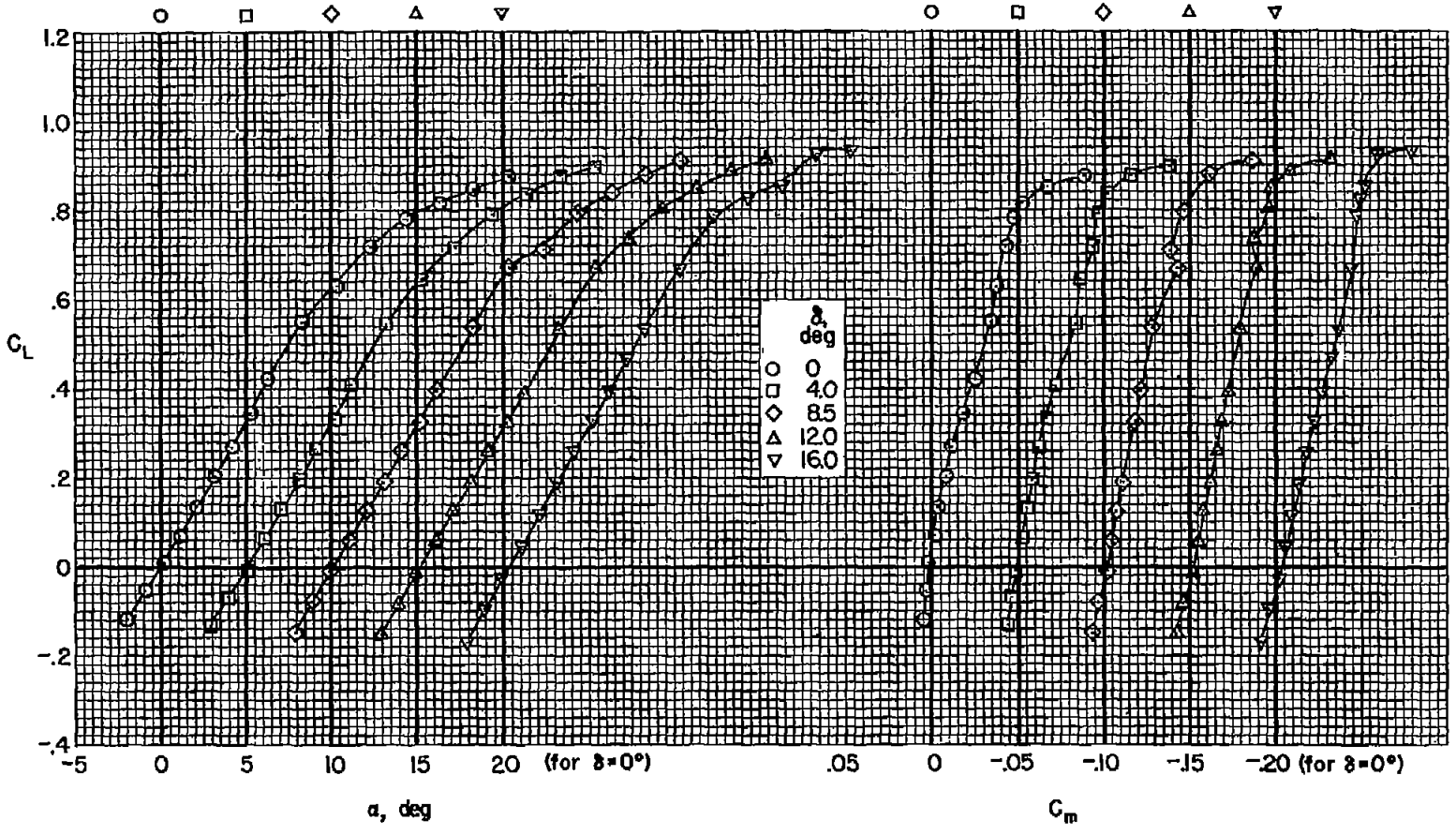

(c) M = 0.80

Figure 9.- Continued.

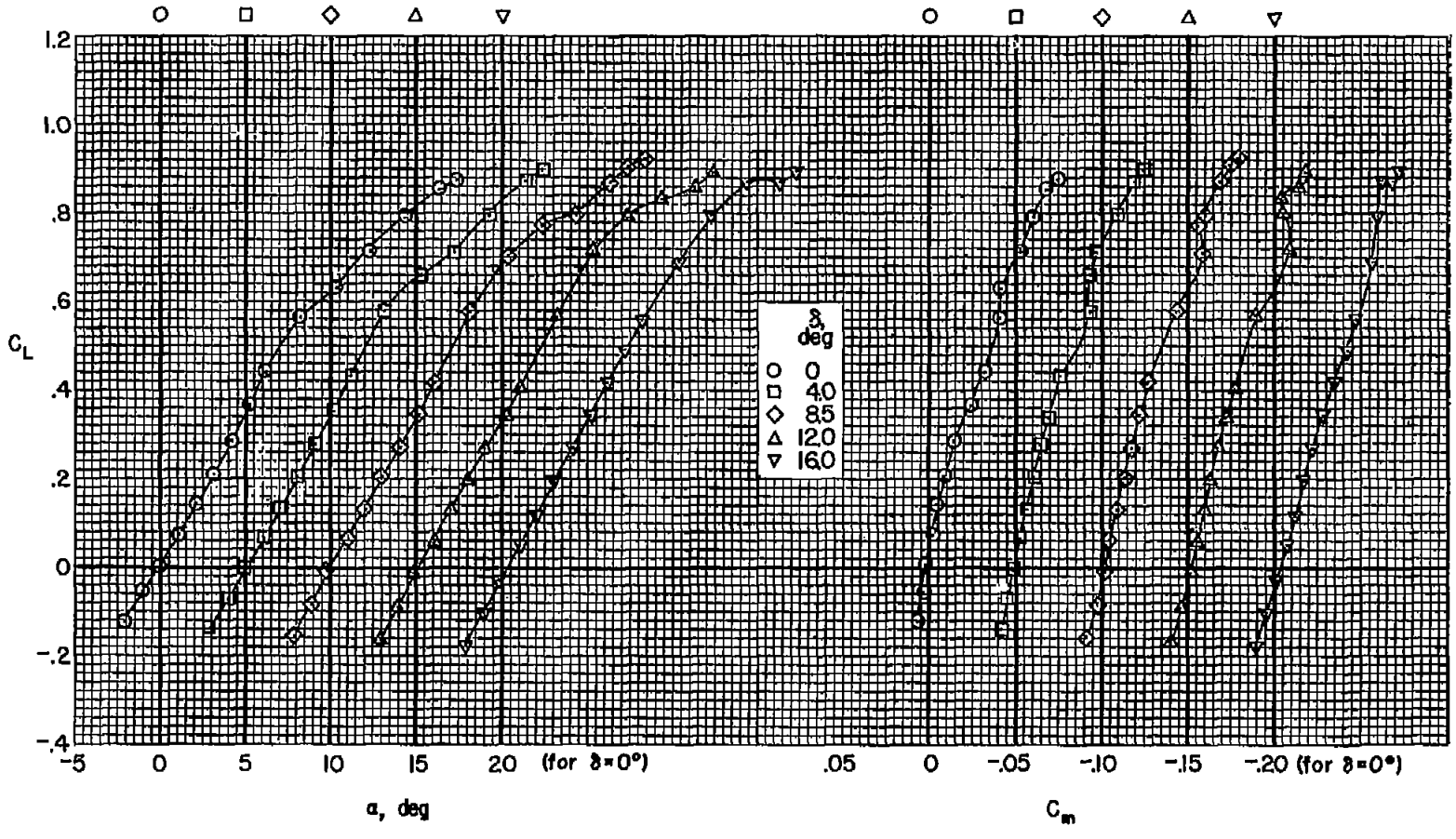

(d) M = 0.85

Figure 9.- Continued.

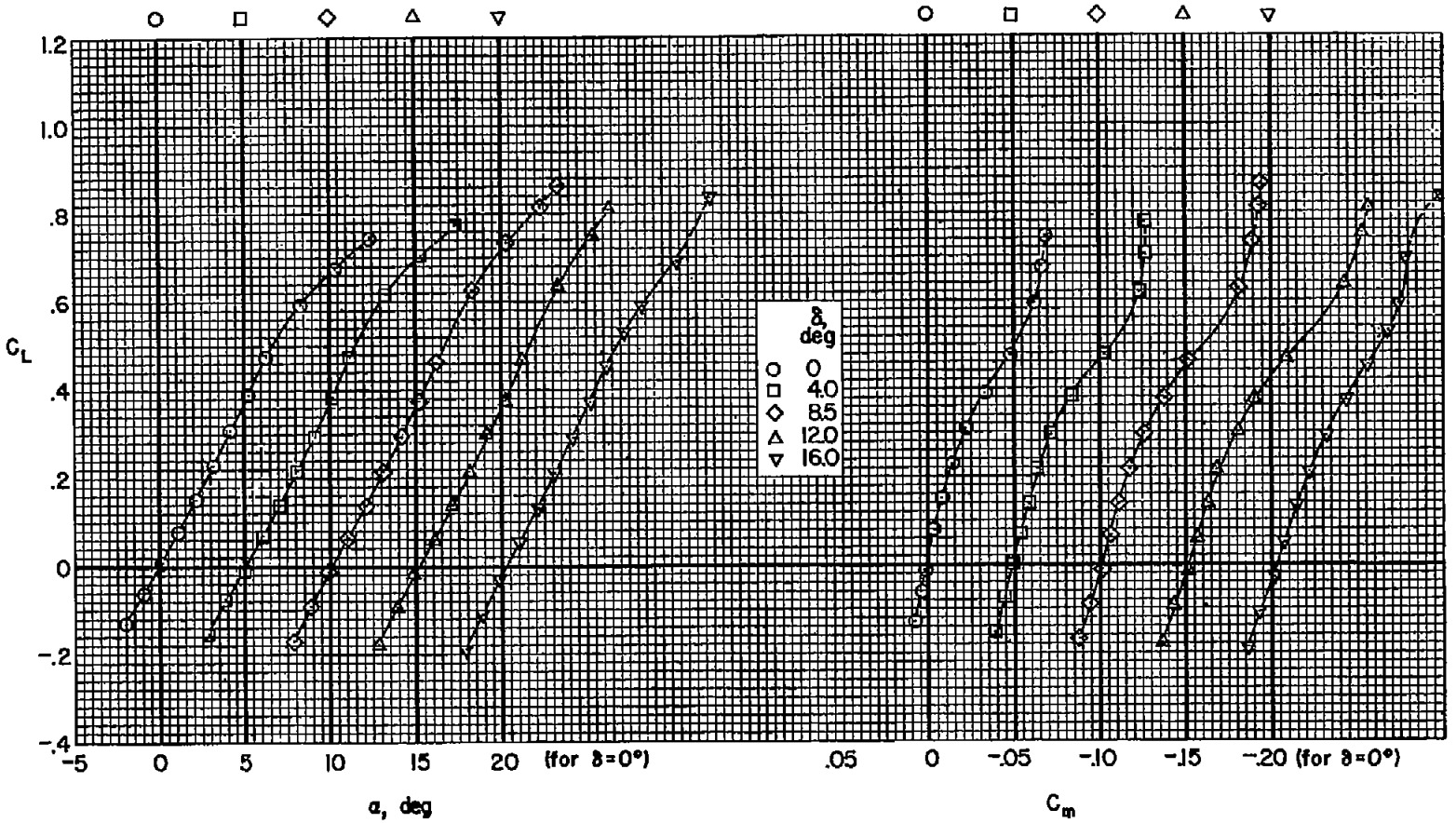

(e) M = 0.90

Figure 9.- Continued.

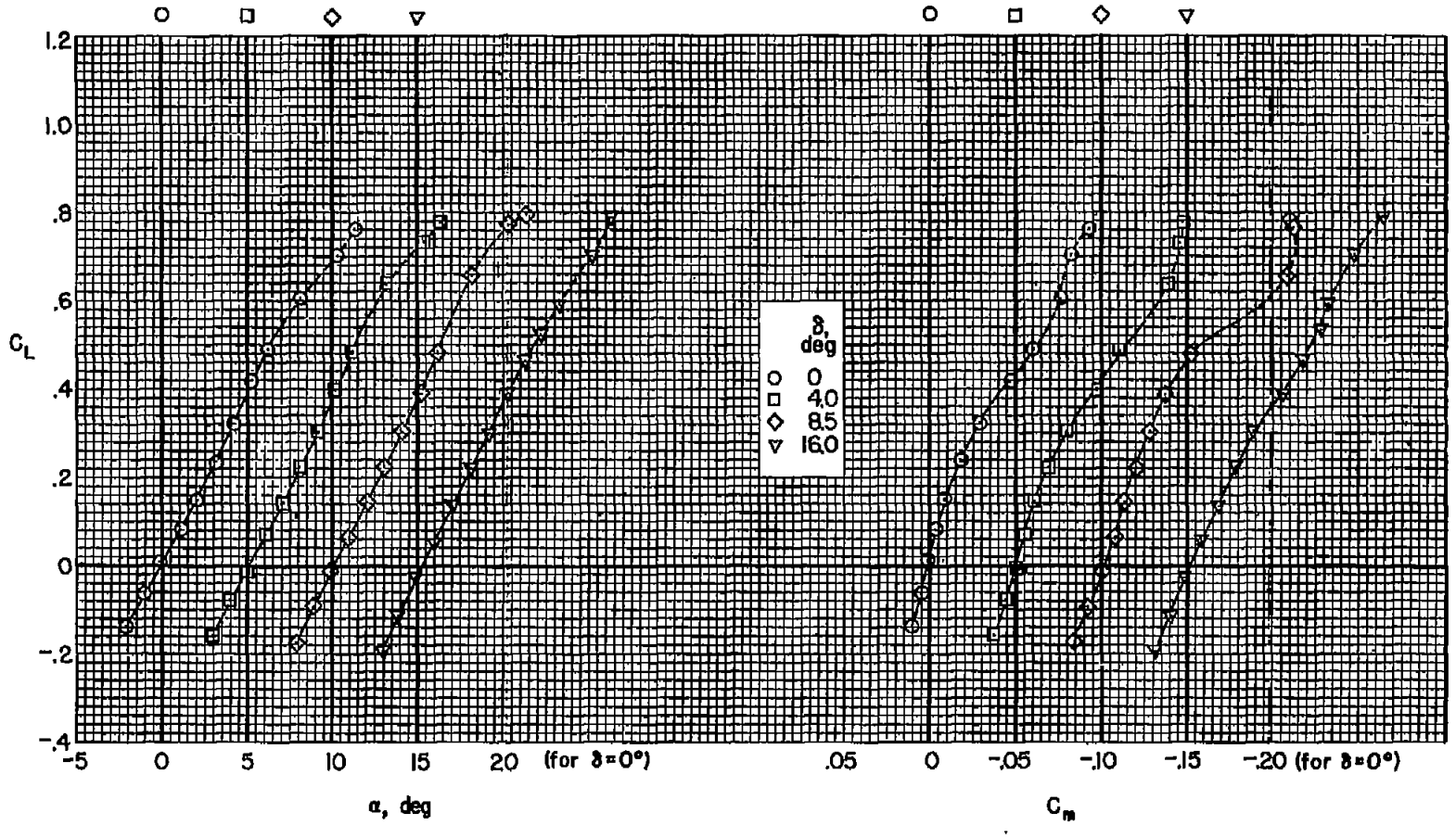

(f) M = 0.92

Figure 9.- Concluded.

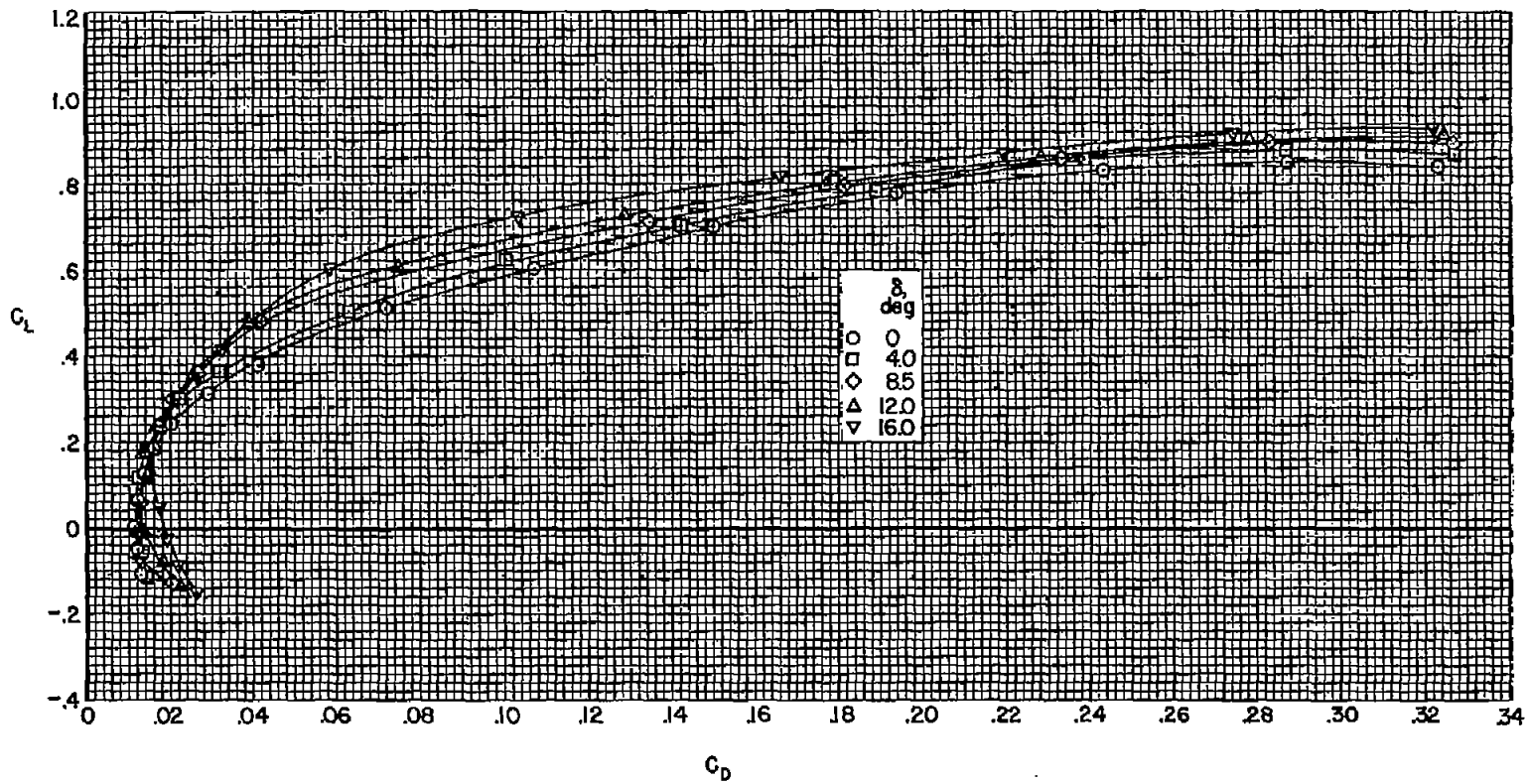

(a) M = 0.60

Figure 10.- The effect of flap deflection on the drag coefficients of the model; wire on, $R = 3.2 \times 10^6$.

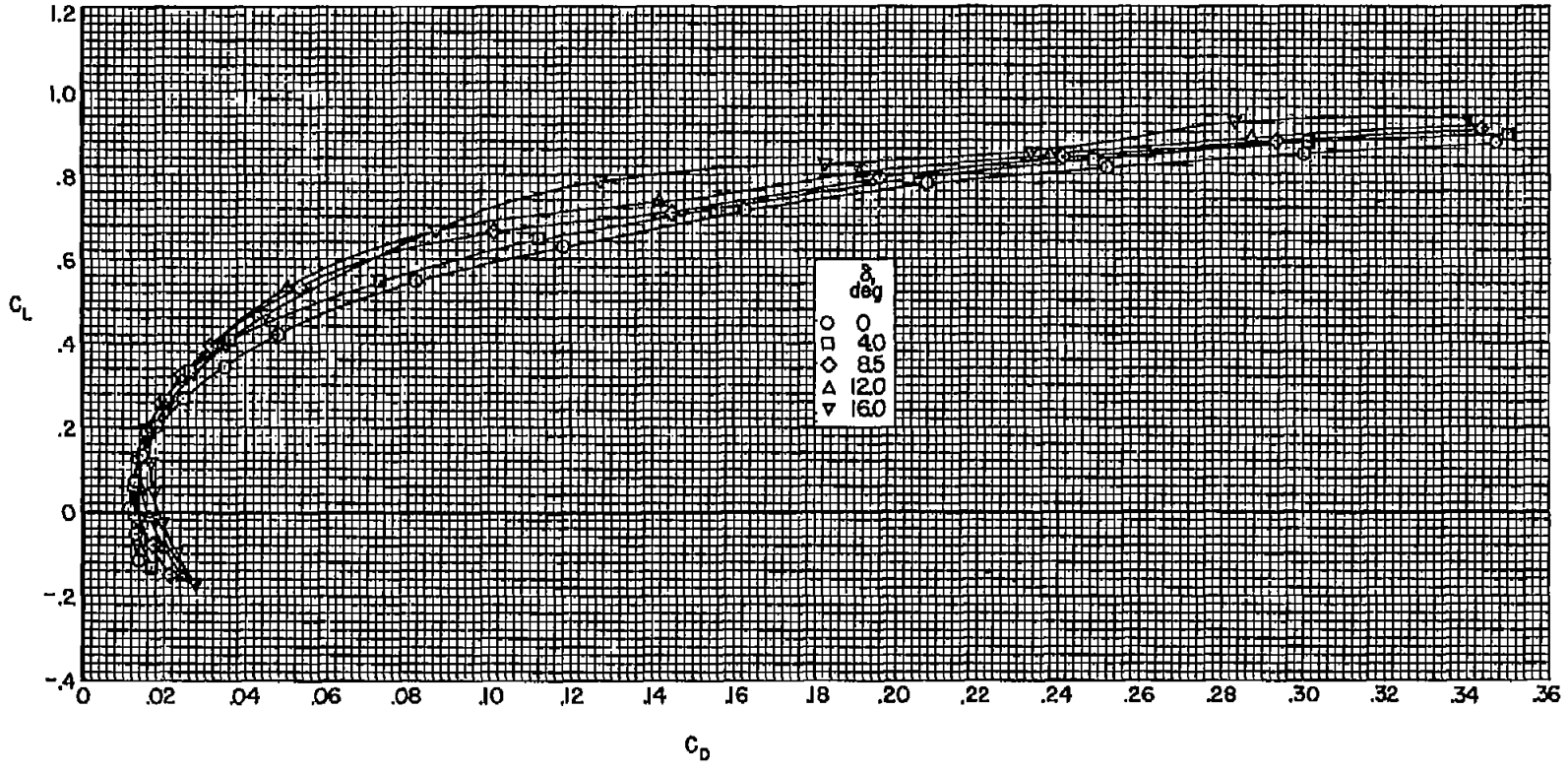

(b) M = 0.80

Figure 10.- Continued.

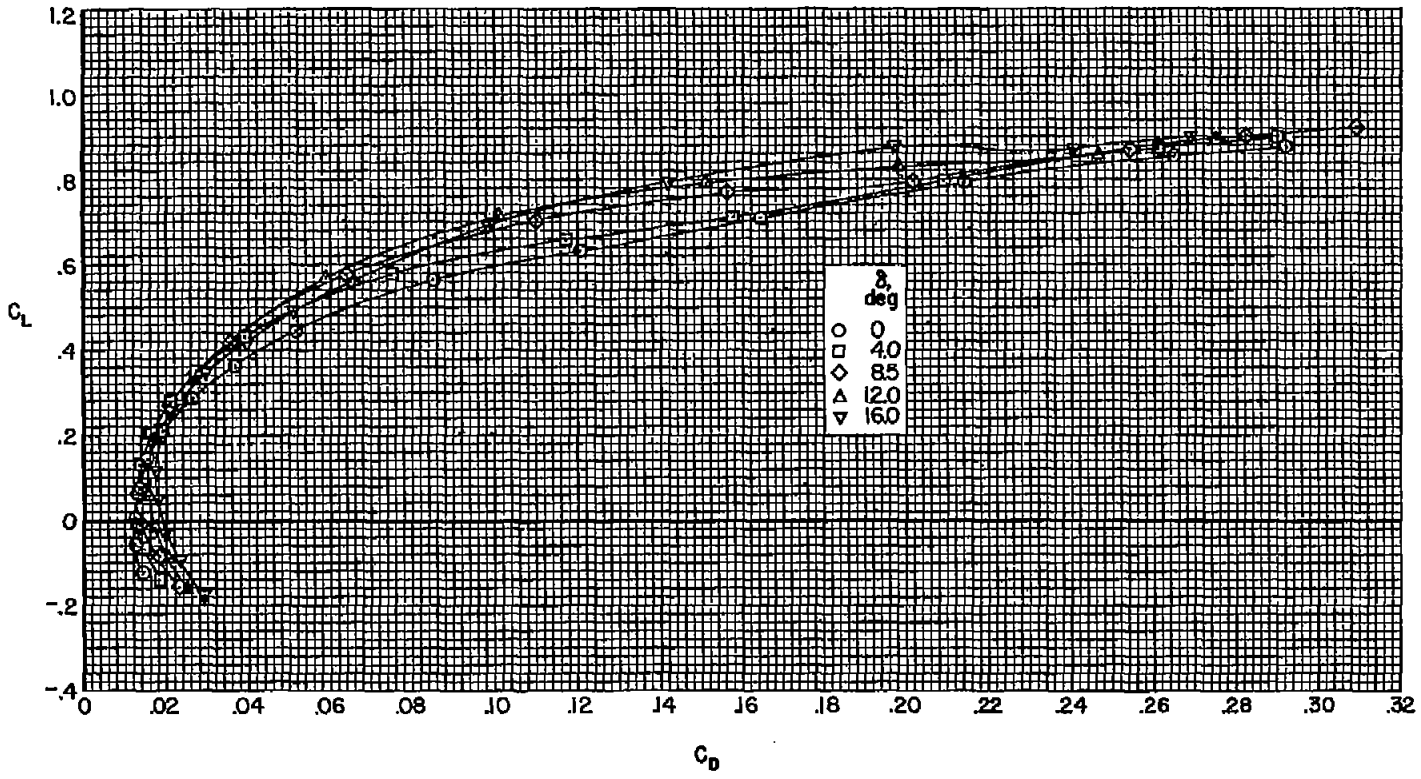

(c) M = 0.85

Figure 10.- Continued.

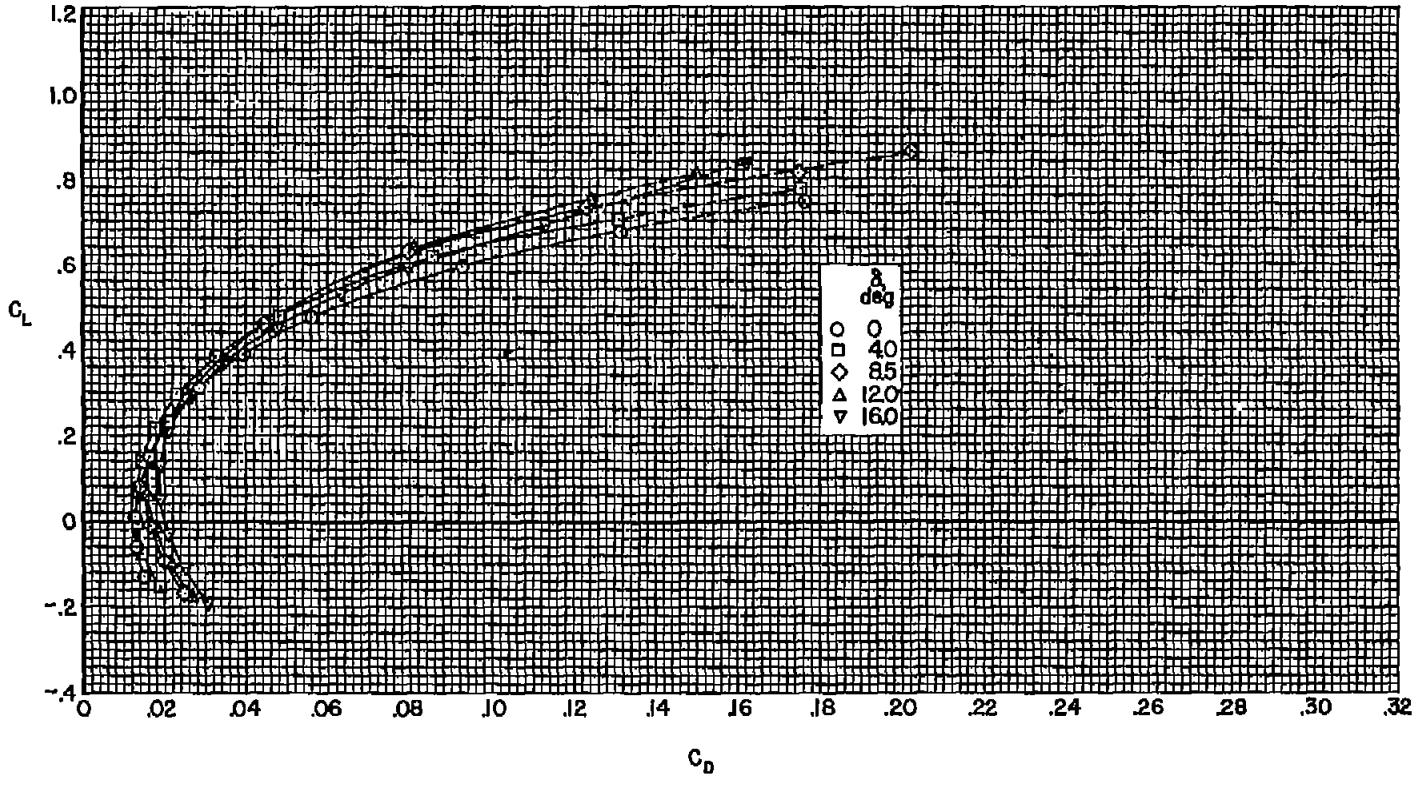

(d) M = 0.90

Figure 10.- Continued.

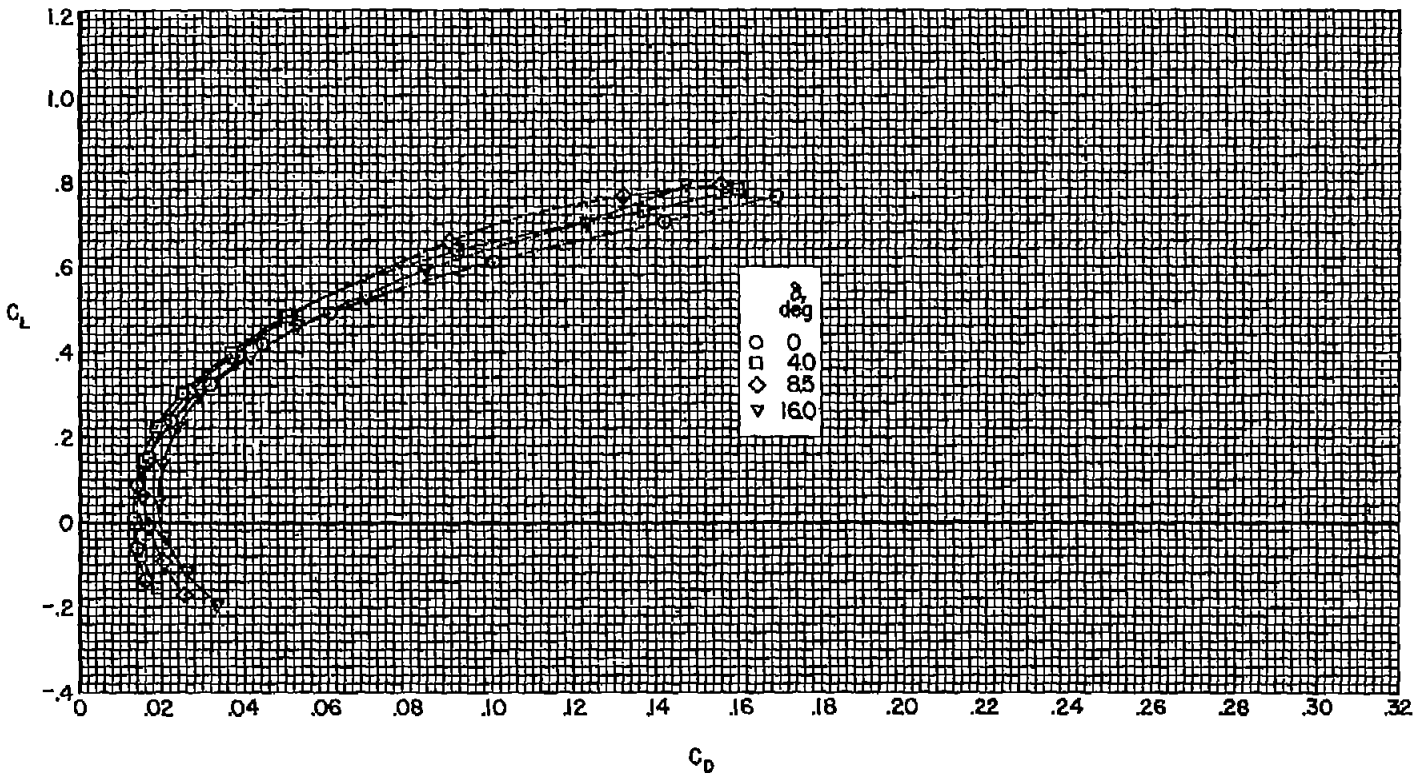

(e) M = 0.92

Figure 10.- Concluded.

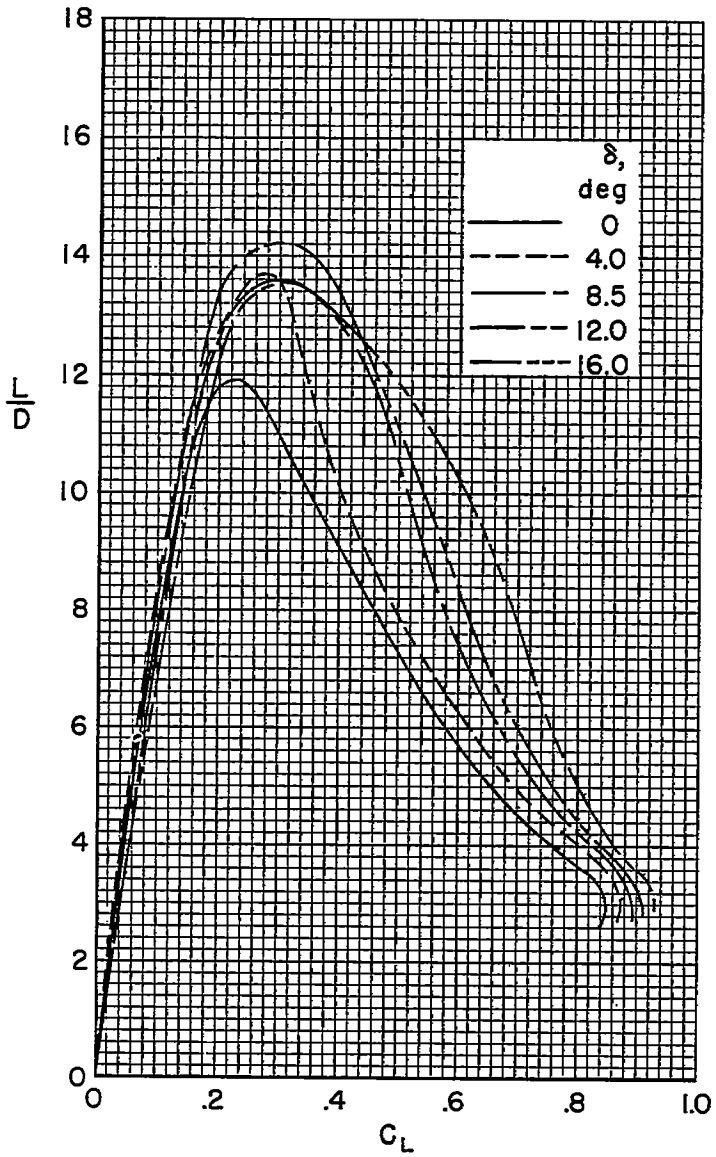

(a) M = 0.60

Figure 11.- The effect of flap deflection on the lift-drag ratios of the model; wire on, $R = 3.2 \times 10^6$.

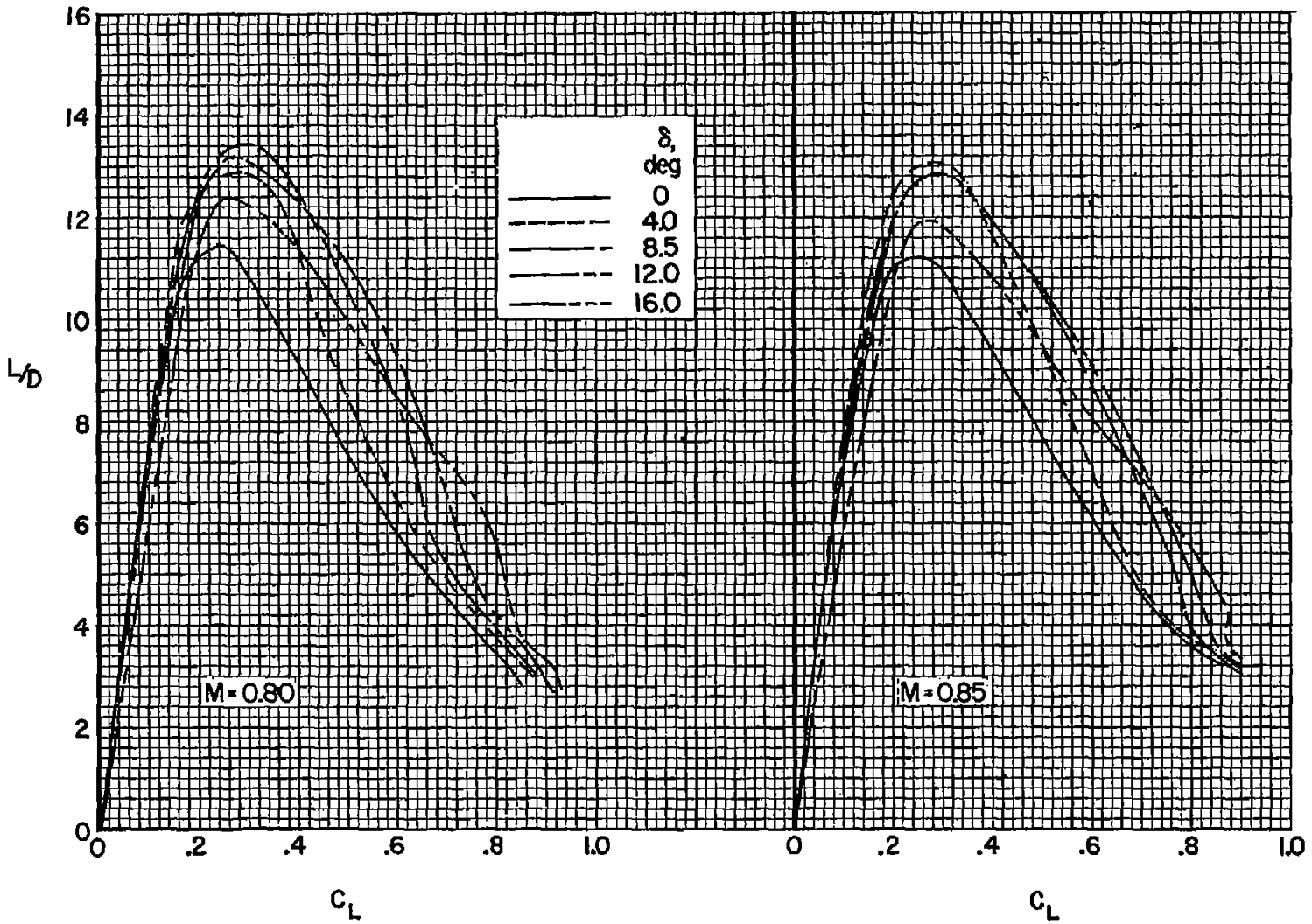

(b) M = 0.80, 0.85

Figure 11.- Continued.

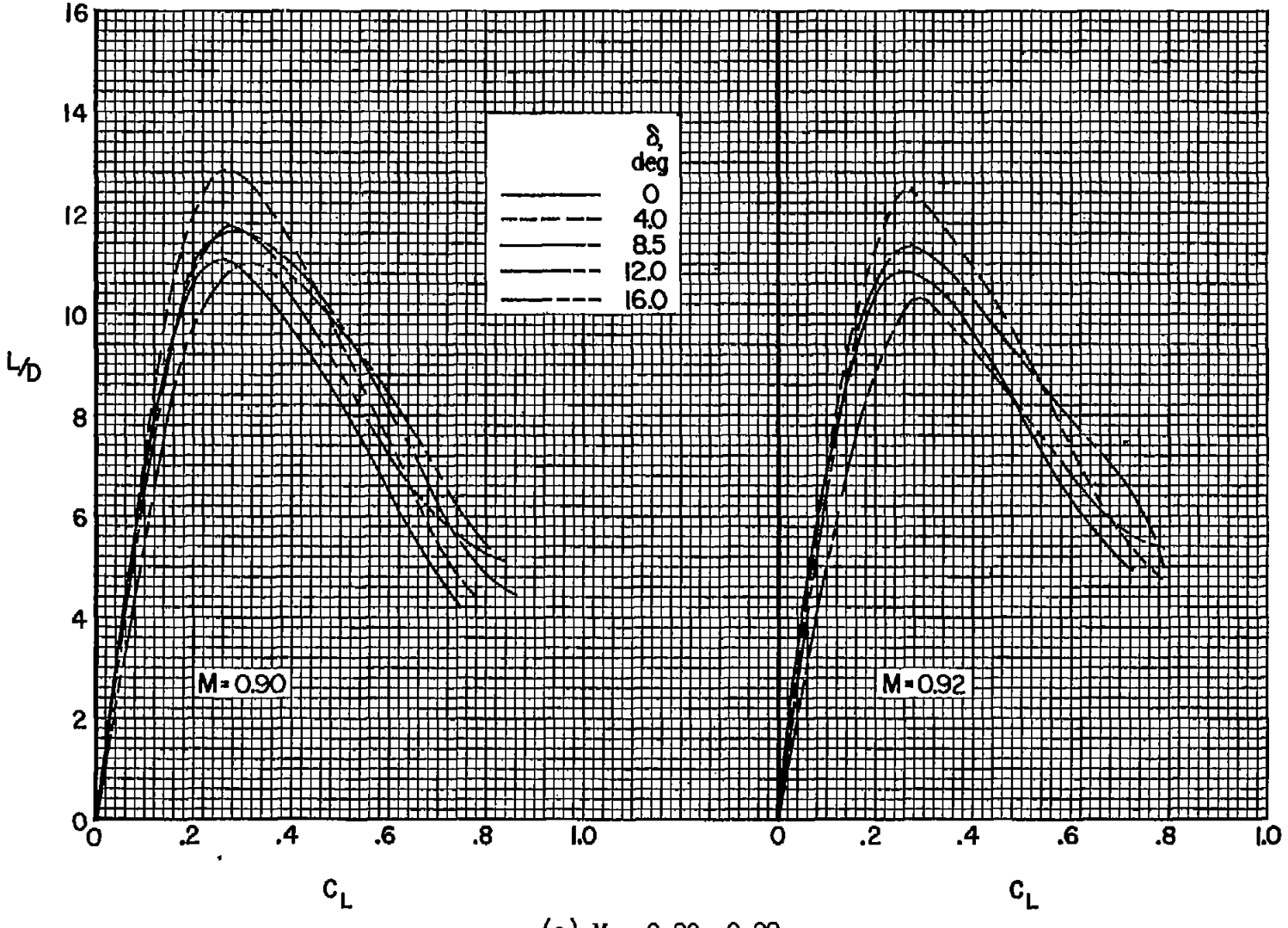

(c) M = 0.90, 0.92

Figure 11.- Concluded.

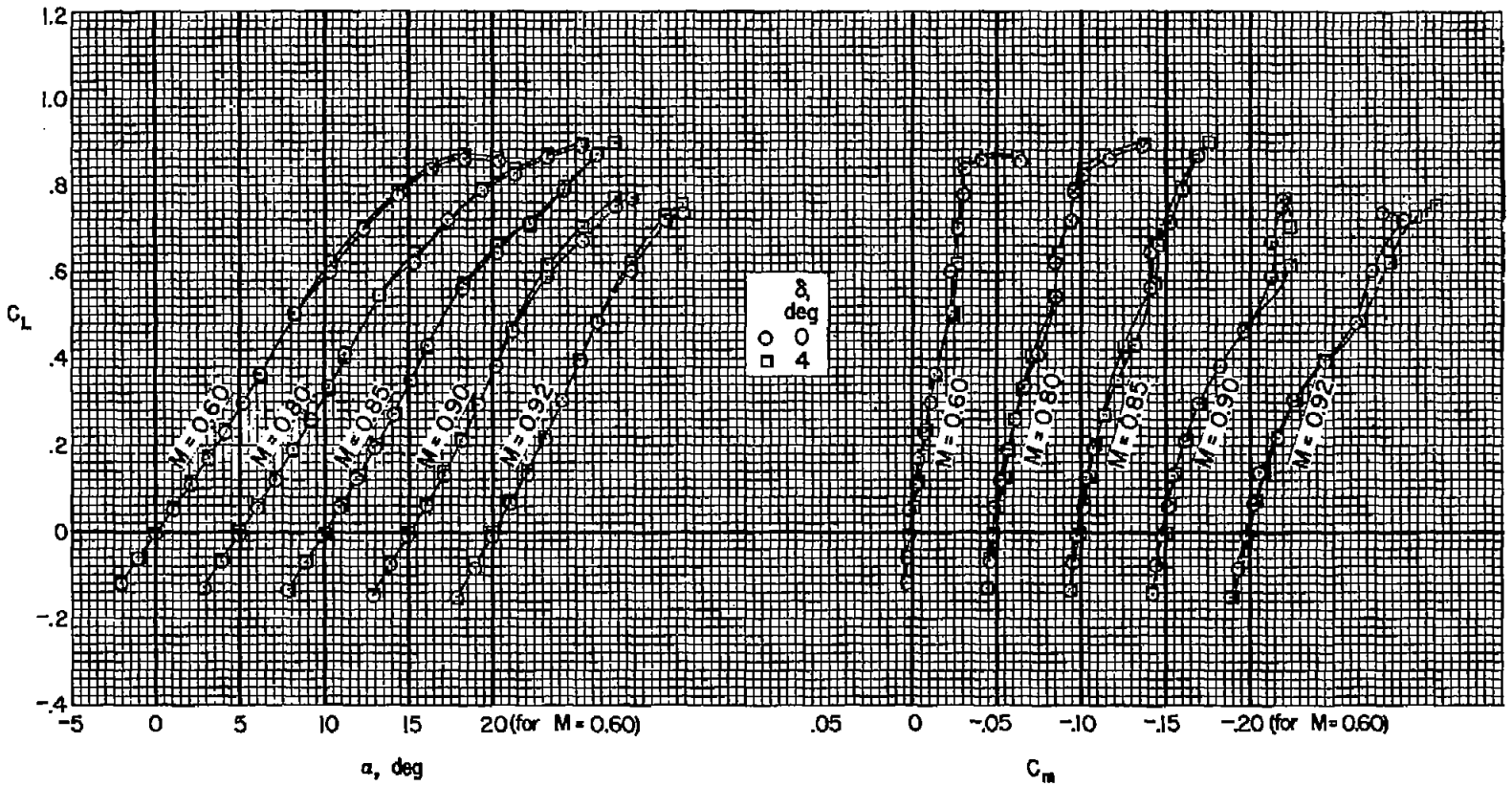

Figure 12.- The effect of Mach number on the lift and pitching-moment coefficients of the model; wire off, R = 3.2×10^6.

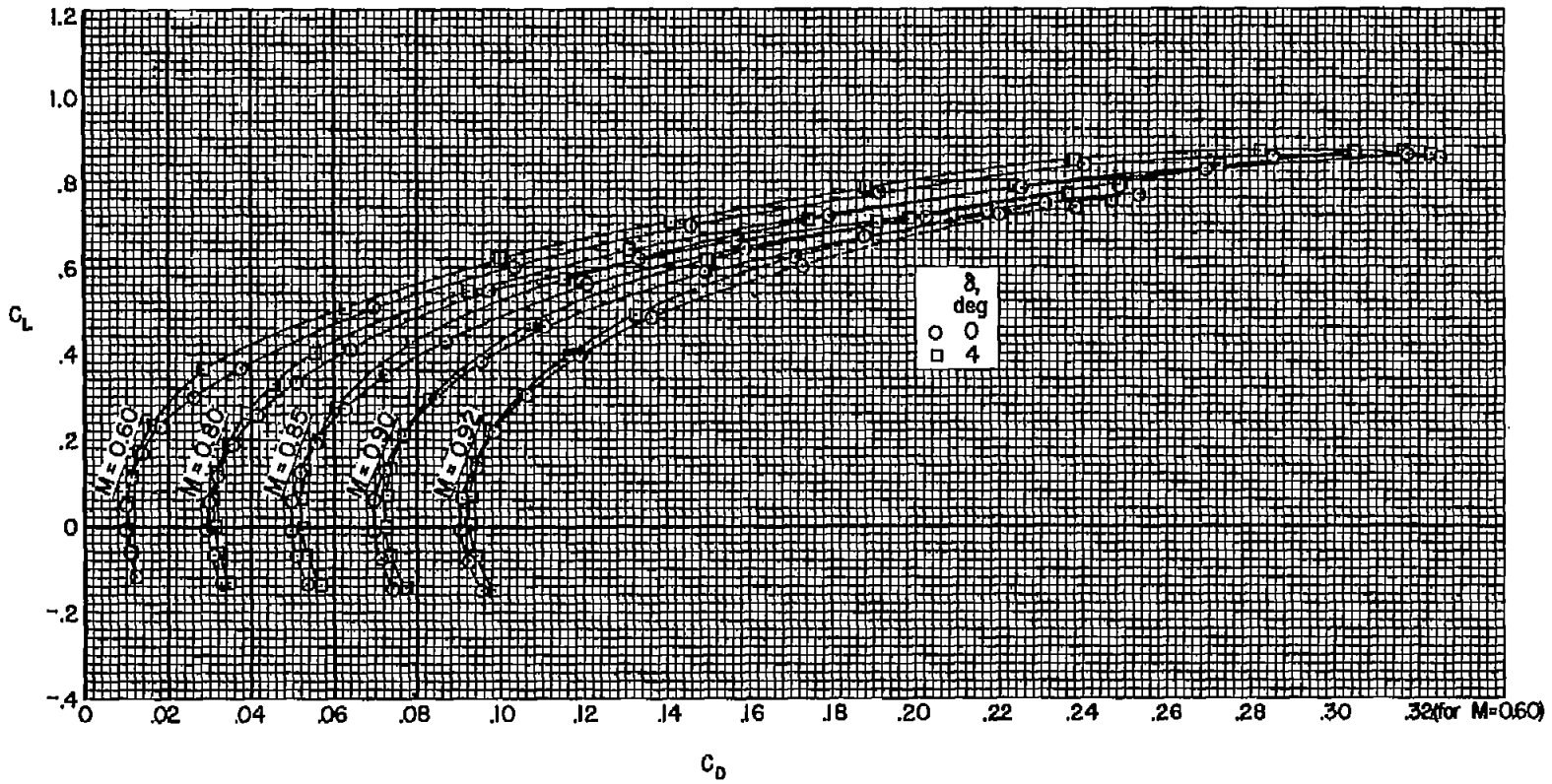

Figure 13.- The effect of Mach number on the drag coefficients of the model; wire off, $R = 3.2 \times 10^6$.

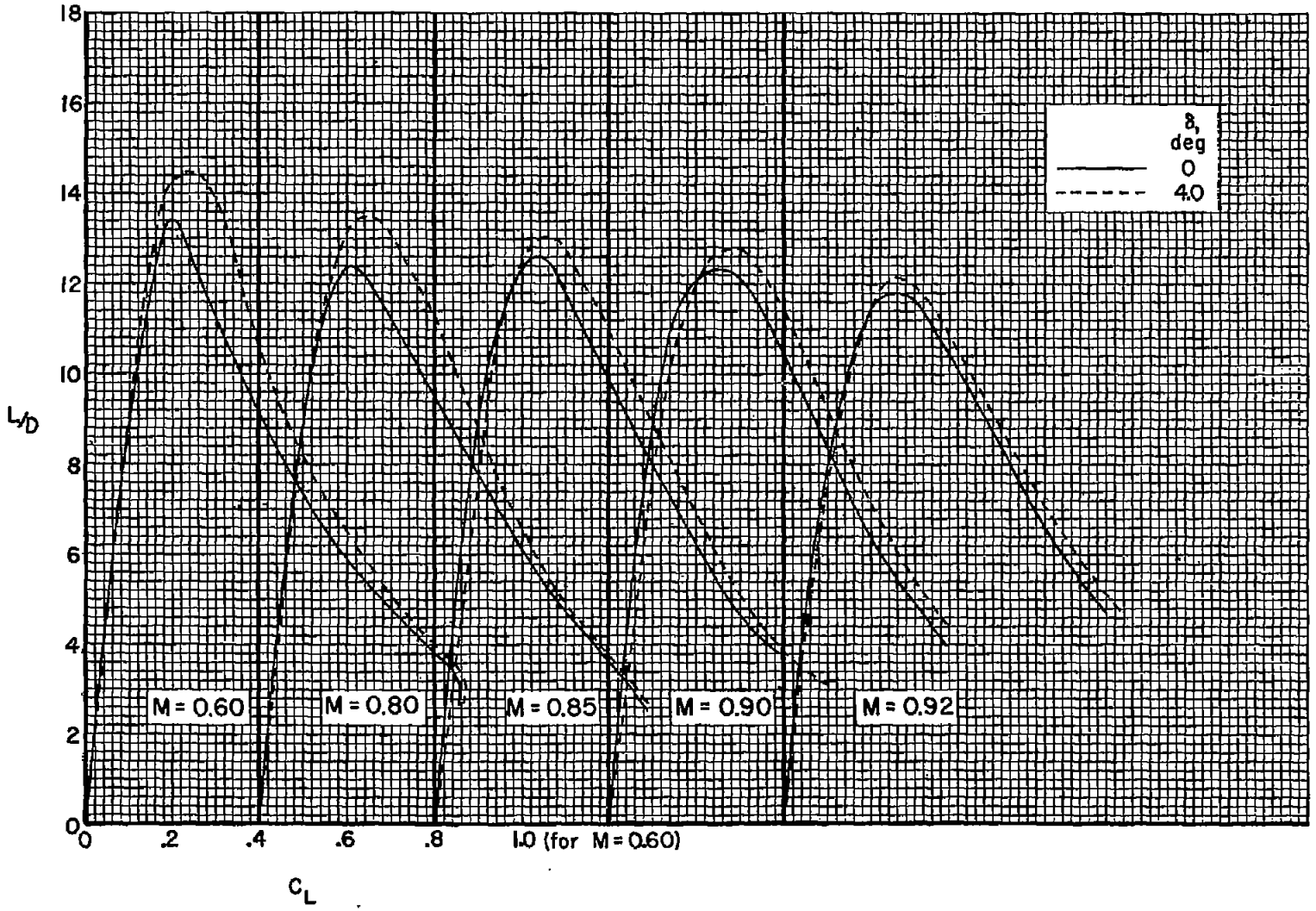

Figure 14.- The effect of Mach number on the lift-drag ratios of the model; wire off, $R = 3.2 \times 10^6$.

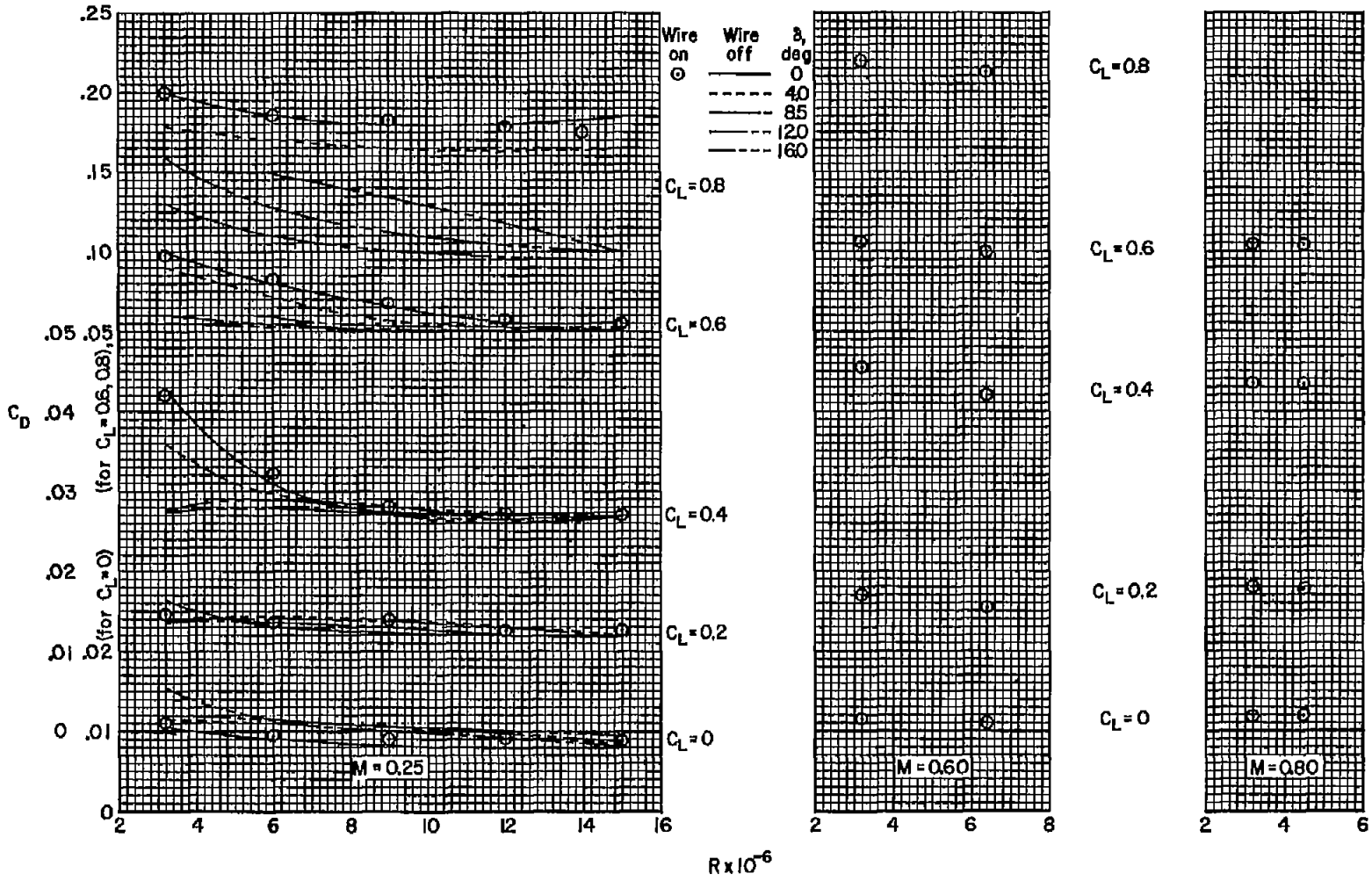

Figure 15.- The variation with Reynolds number of drag coefficient at constant lift coefficient.

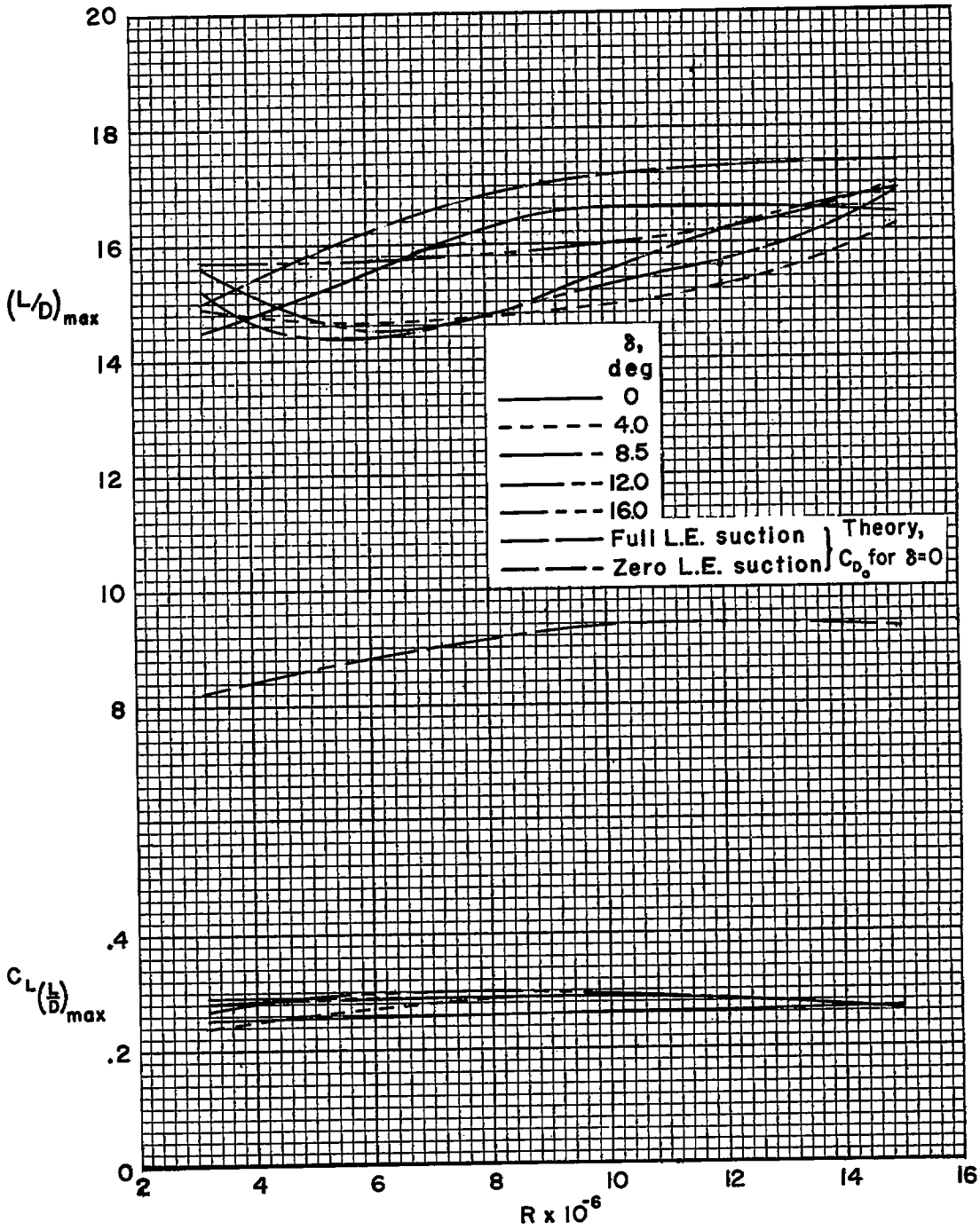

Figure 16.- The effect of flap deflection on the variation with Reynolds number of maximum lift-drag ratio and lift coefficient for maximum lift-drag ratio; wire off, M = 0.25.

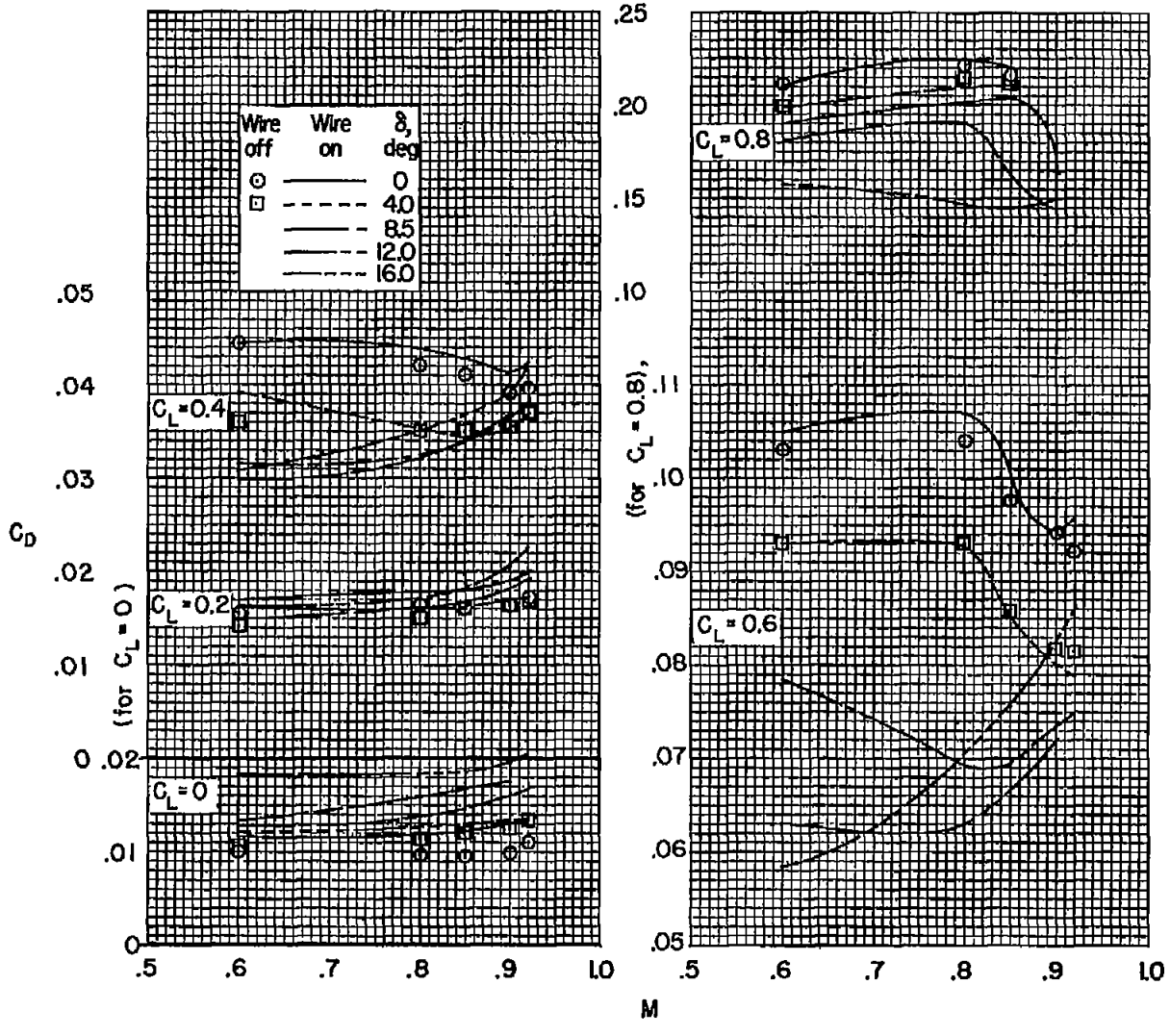

Figure 17.- The effect of flap deflection on the variation with Mach number of drag coefficient at constant lift coefficient; $R = 3.2 \times 10^6$.

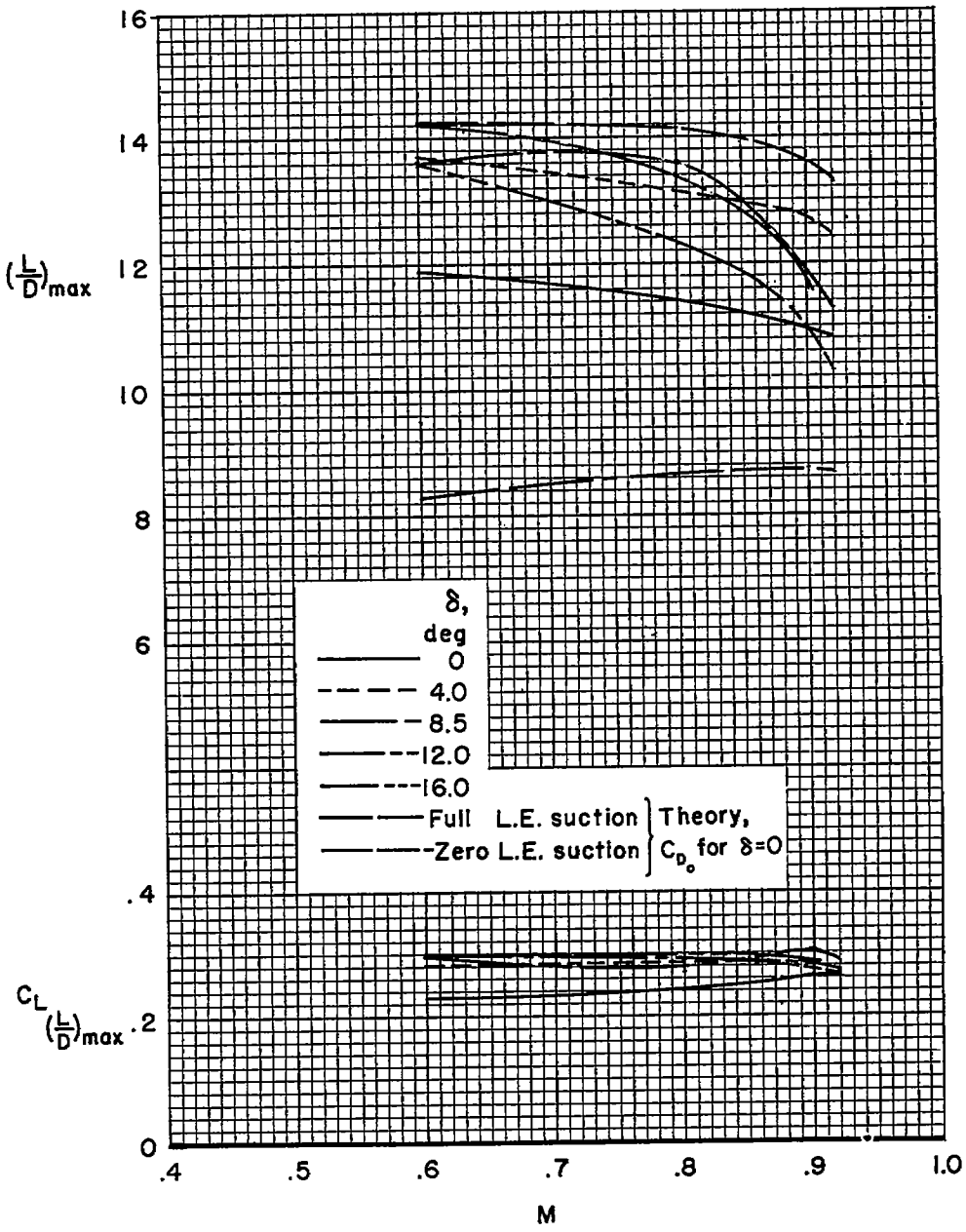

Figure 18.- The effect of flap deflection on the variation with Mach number of maximum lift-drag ratio and lift coefficient for maximum lift-drag ratio; wire on, $R = 3.2 \times 10^6$.

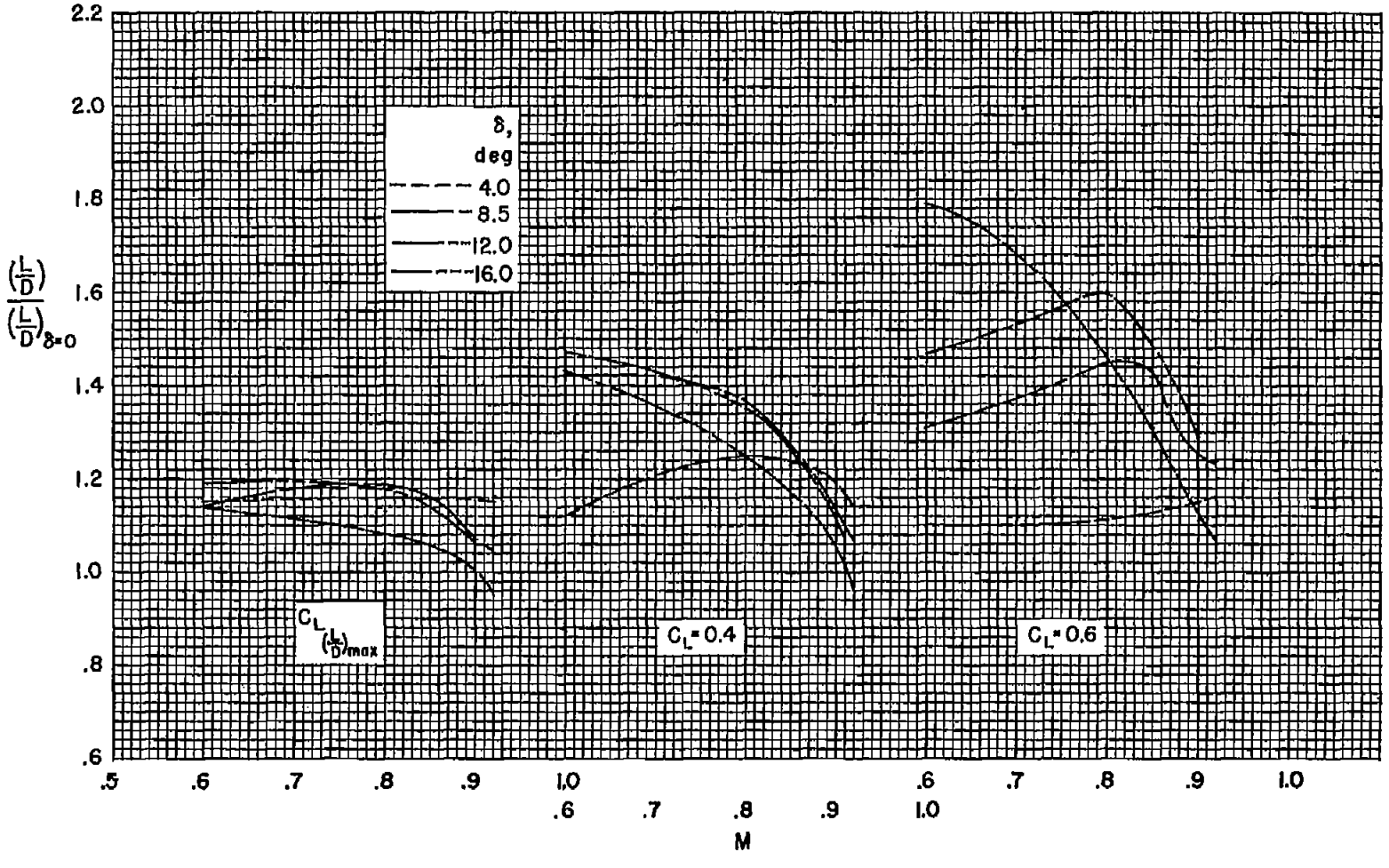

Figure 19.- The variation with Mach number of the increase in lift-drag ratio due to flap deflection; wire on, $R = 3.2 \times 10^6$.

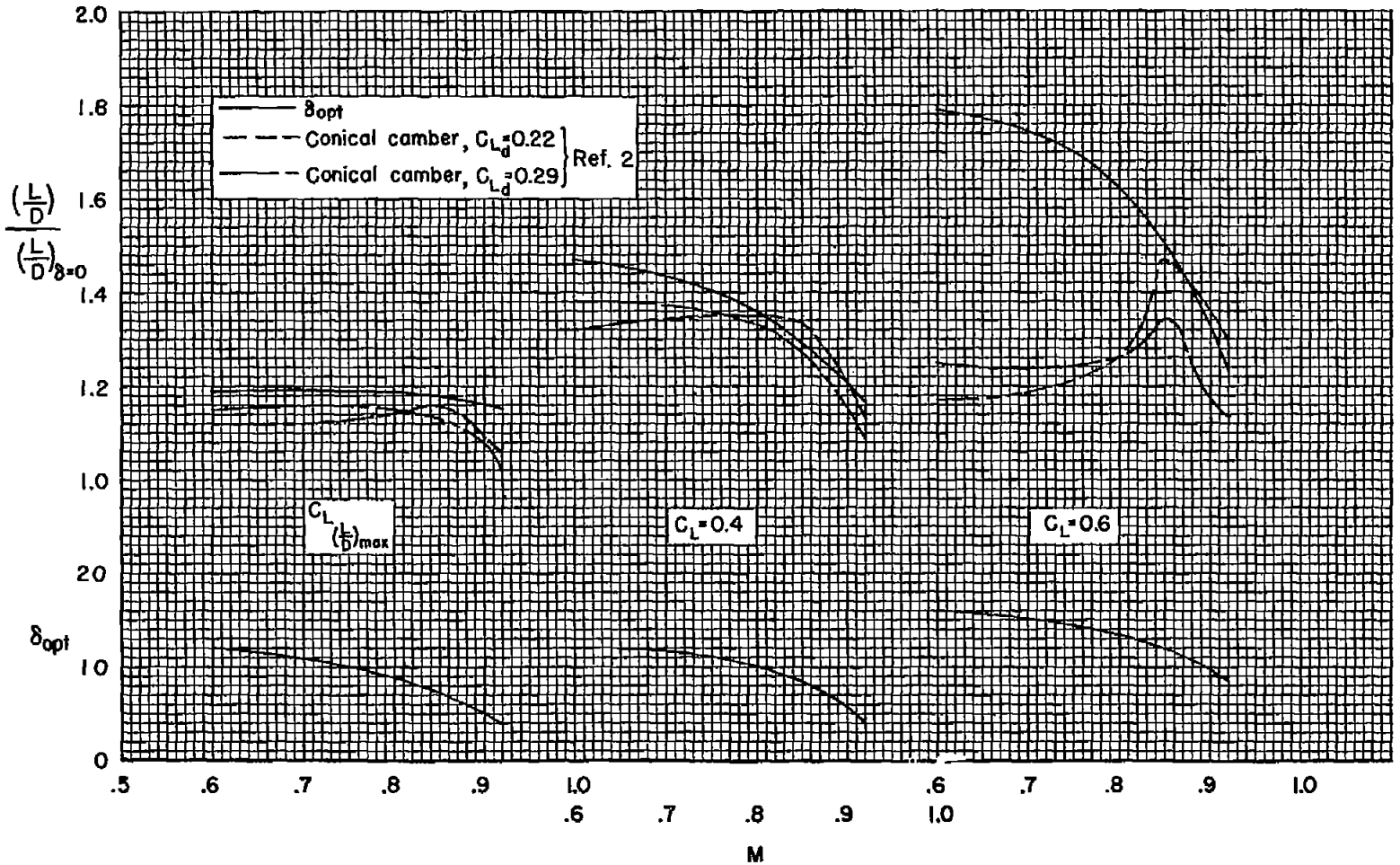

Figure 20.- Comparison of the increase in lift-drag ratio due to optimum flap deflection with that due to conical camber; wire (or roughness) on.

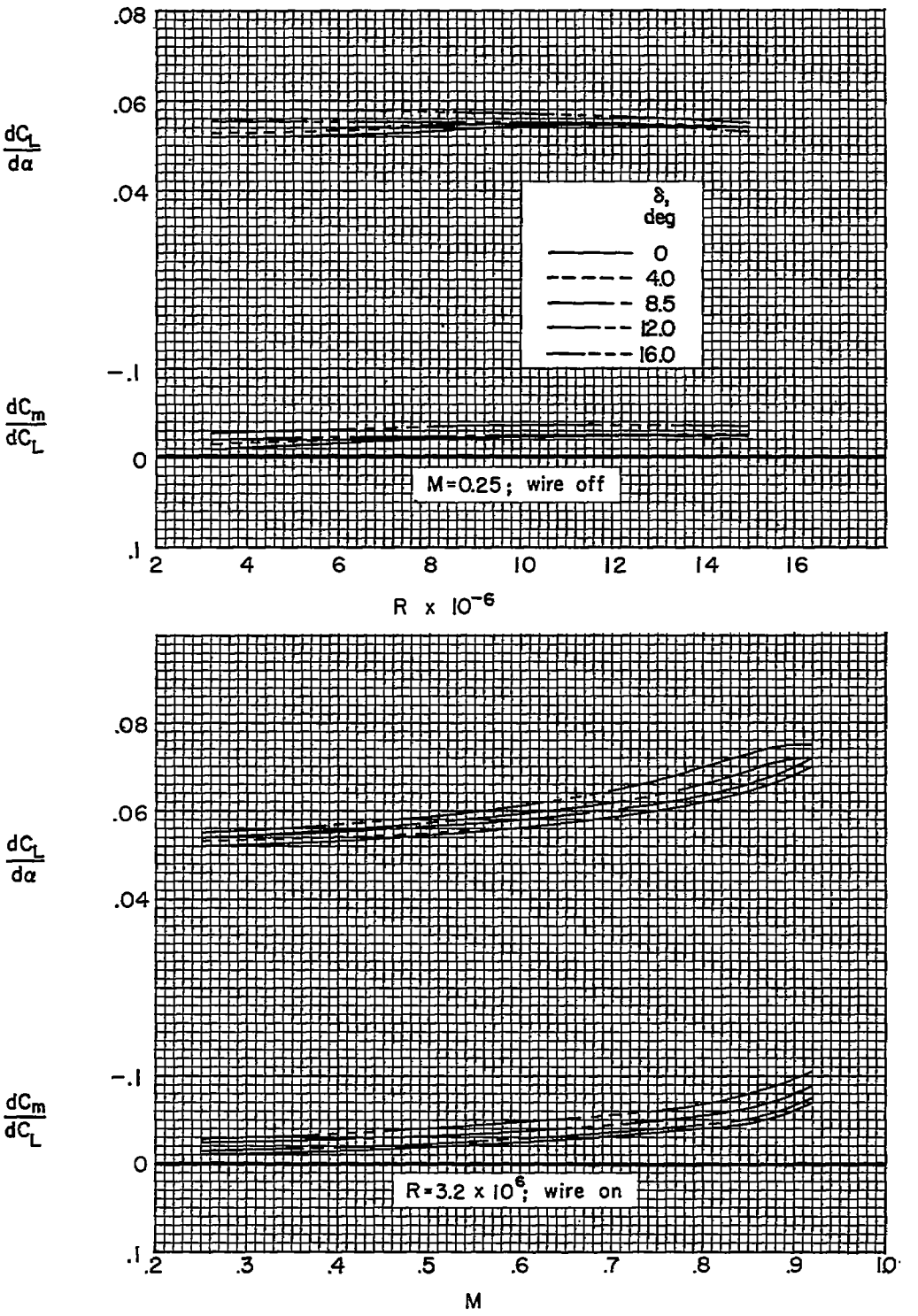

Figure 21.- The effect of flap deflection on the variation with Reynolds number and Mach number of lift- and pitching-moment curve slopes.

NACA - Langley Field, Va.